Handbook of Heterogeneous Catalysis, Vol.3, (2008) 1492-1516

5.2.7. Nonlinear Dynamics: Oscillatory Kinetics and Spatio-Temporal Pattern Formation

G. Ertl

5.2.7.1 Introduction

The rate of a catalytic reaction is governed by the underlying mechanism, i.e. the sequence of elementary reaction steps, and depends on the external control parameters such as the concentrations (= partial pressures) p_j of educt and product species and temperature T, if transport processes are excluded in this context. More specifically, usually the adsorbed species are assumed to be randomly distributed over the surface, and their concentrations (= coverages) θ_i are described within a mean-field approximation so that the reaction rate (= number of molecules r formed per unit time, dn_r/dt_t) is given by

$$\frac{dn_r}{dt} = f(\theta_i, T) \quad (1)$$

whereby the coverages θ_i are in turn determined by a set of differential equations (modeling the individual steps of adsorption, desorption and surface reaction) of the type

$$\frac{d\theta_i}{dt} = g_i(p_j, \theta_i, T) \quad (2)$$

Proper treatment then requires that additional constraints given by heat and mass balance are taken into consideration.

Under flow conditions with the external control parameters being kept fixed, usually the reaction proceeds at steady state with constant rate, i.e., dn_r/dt = constant and $d\theta_i/dt = 0$. Due to the nonlinear character of the quoted differential equations, this has, however, not necessarily to be the case; the kinetics may – for certain ranges of parameters – become oscillatory or even irregular (chaotic). Such systems are typically far away from equilibrium, and as a consequence "dissipative structures" [1] may emerge. The coverages θ_i may vary both in time and space and may give rise to phenomena of spatio-temporal self-organization as being treated in the general area of nonlinear dynamics [2].

Experimental observations on oscillatory kinetics have been made with quite different systems, first with electrochemical reactions [3] and later quite extensively in homogeneous solution with the famous Belousov-Zhabotinsky (BZ) reaction and related systems [4, 5]. In heterogeneous catalysis, rate oscillations were first reported around 1970 by Wicke and co-workers for the oxidation of carbon monoxide on supported platinum catalysts [6, 7]. Since then numerous catalytic reaction systems have been investigated in more or less detail, and this subject has also been reviewed quite extensively [8–17]. Oscillatory kinetics have so far been found with more than a dozen catalytic reactions, in particular with CO oxidation, but also with oxidation of H_2, NH_3, or hydrocarbons, with reduction of NO or N_2O by CO, H_2, or NH_3, as well as with hydrogenation reactions and even with the endothermic decomposition of methyl amine. Further distinction is made with respect to the type of catalyst (e.g. single crystal or polycrystalline material) as well as the pressure range studied. This classification is reasonable for the following reasons:

(i) By far the most detailed insights into the underlying mechanisms and the general phenomenology of spatio-temporal self-organization were obtained in studies with well-defined single crystal surfaces by applying the arsenal of modern surface physical methods.

(ii) Single crystal studies are usually conducted with bulk samples under low pressure conditions ($\leq 10^{-4}$ mbar) where the temperature changes associated with varying reaction rate are negligible. In addition, the mean-free path of gaseous molecules is comparable or even larger than the dimensions of the reaction vessel, which is operated as a continuous flow reactor. Hence, concentration gradients in the gas phase are practically instantaneously ($\leq 10^{-3}$ s) transmitted. Analysis of such experiments is thus appreciably simplified.

(iii) Experiments with polycrystalline, i.e. “real”, catalysts are usually conducted at elevated partial pressures ($\geq$ 1 mbar) under which the heat released by the reaction may lead to noticeable temperature variations. The resulting thermokinetic effects may become dominating, so that even the nonuniformity of the surface chemistry is masked and quite novel phenomena may arise. Ideally, the reaction is conducted in a way, which may be described by a continuously stirred tank reactor (CSTR), i.e., perfect mixing ensures that the concentrations are everywhere identical. However, frequently a concentration profile exists along the reactor, which is hence rather of the plug-flow type. It is thus evident that heat and mass transfer limitations may play important roles with such systems.

Generally, an extended system such as a single crystal surface, or even more a supported catalyst, exhibiting temporal variations of the integral reaction rate has to be subject to a coupling mechanism between various parts. Otherwise, superposition of the uncorrelated contributions from different regions would cause averaging so that constant steady-state behavior would result. As a consequence, the coverages θ_i as introduced in Eqs. (1) and (2) will in general not only depend on time but also on spatial coordinates, and proper mathematical modeling will be achieved in terms of partial differential equations (PDE) as will be outlined further below.

The following coupling mechanisms may be operating:

(i) *Surface diffusion* Local differences of the coverages will lead to surface diffusion of the adsorbates, and inclusion of this effect into mathematical modeling extends Eq. (2) to reaction-diffusion (RD) equations of the type

$$\frac{\mathrm{d}\theta_i}{\mathrm{d}t} = g_i\left(p_j, \theta_i, T\right) + D_i \nabla^2 \theta_i \qquad (3)$$

where D_i is the diffusion coefficient of the respective adsorbed species. Diffusion lengths of the systems under consideration here are typically of the order of about 1 μm. Concentration patterns will hence be formed on extended single crystal surfaces, but also on monolithic polycrystalline material where the individual grains have typically much larger diameters [18]. However, other types of RD phenomena will develop on the small (≤ 10 nm) crystal planes of supported catalyst particles as modeled in experiments with field emission tips [19, 20].

(ii) *Gas-phase coupling* Varying reactivity will also affect the partial pressures of the reactants, even in a flow system. As outlined above, at low pressures these changes will propagate practically instantaneously and may offer a rather effective "global" coupling mechanism, which synchronizes different parts of a single crystal surface or even of separated samples [21]. Experiments with external periodic modulation of one of the partial pressures revealed that indeed amplitudes far below 1% may suffice to cause such synchronization effects [22]. At elevated pressures, however, this coupling mechanism will be of minor importance.

(iii) *Heat conductance* Local variations of reactivity will be accompanied by temperature differences due to the finite reaction enthalpies. Coupling between different regions may thus occur through heat flux counterbalancing the temperature gradients. This mechanism generally prevails at higher pressures and also with supported catalysts, where temperature changes of up to the order of 100 K may arise. The characteristic "diffusion" length is in this case of the order of about 1 mm, which is much larger than the mean separation between catalyst particles or even the diameters of their individual crystal planes. As a consequence, such a system may again be regarded as being uniform (on the relevant length scale), but the observed phenomena will be strongly affected by these heat phenomena rather than by the details of the surface chemistry, and external constraints (such as a constant average temperature) may provide efficient global coupling.

In the following, the $H_2 + O_2$ reaction on a Pt(111) surface will first serve to demonstrate how observations on the atomic scale (by scanning tunneling microscopy) enabled direct insight into the coupling between elementary surface reactions and adsorbate diffusion, leading to spatio-temporal pattern formation on mesoscopic scale and thus permitting modeling on the continuum level by mean-field approximations as sketched before. Next, the theoretical background resulting from this approach will be briefly outlined.

No attempt will be made to present an extended review of the experimental and theoretical results from this still rapidly growing field, but instead the principle effects will be illustrated by selected examples with progressing complexity.

5.2.7.2 From the Atomic to the Mesoscopic Scale: Spatio-temporal Self-organization in the Catalytic Oxidation of Hydrogen on a Pt(111) Surface

The observation that platinum caused hydrogen to react with oxygen to give water "by mere contact" was already made in 1823 by Döbereiner [23], but its mechanism could be fully explored only recently [24]. Both O_2 and H_2 are dissociatively adsorbed. The recombination between O_{ad} and H_{ad} yields OH_{ad} which is a relatively slow step.

Considerably more efficient is the reaction $O_{ad} + H_2O_{ad} \rightarrow 2OH_{ad}$, from where the reaction is completed via $OH_{ad} + H_{ad} \rightarrow H_2O_{ad}$.

Figure 1 shows a series of successive STM images from a Pt(111) surface which had been precovered with O_{ad} and was then exposed to a continuous flow of H_2. The first three frames were taken at 8 x 10^{-9} mbar H_2 and 131 K with atomic resolution and show how the dark dots representing O_{ad} (A) are at first transformed into OH_{ad} patches (B) which are fully developed in (C) from where fuzzy patches of H_2O are formed. The second series of frames were taken on a larger scale at 2 x 10^{-8} mbar H_2 at 112 K and demonstrate the operation of an autocatalytic reaction sequence: The bright dots are nuclei of the OH_{ad} patches whose concentration is locally enhanced by the reaction $O_{ad} + 2H_2O_{ad} \rightarrow 2OH_{ad}$, leading to the formation of a ring-like concentration wave moving outwards into the O_{ad}-rich region leaving the product H_2O_{ad} behind which diffuses under the influence of its concentration gradient from the H_2O-rich to the O-rich zone through the wall of enhanced OH concentration. (Actually this is not a pure OH_{ad}-phase, but rather a mixed OH-H_2O phase as shown by recent experimental [25 - 27] studies). Numerical solution of the set of partial differential equations describing the kinetics of the indicated reaction steps with the inclusion of diffusion of adsorbed H_2O reproduced indeed the experimental data of Fig. 1 qualitatively well, both with respect to the (mesoscopic) length scale and the front velocity, and thus demonstrate that this mean-field approach provides an adequate theoretical description [28]. Other approximations starting with the atomic picture of individual particles are based on Monte Carlo techniques and were applied in a number of studies [29, 30], but will no further be outlined here. Because of the required large size of the lattice computational capabilities present severe limitations.

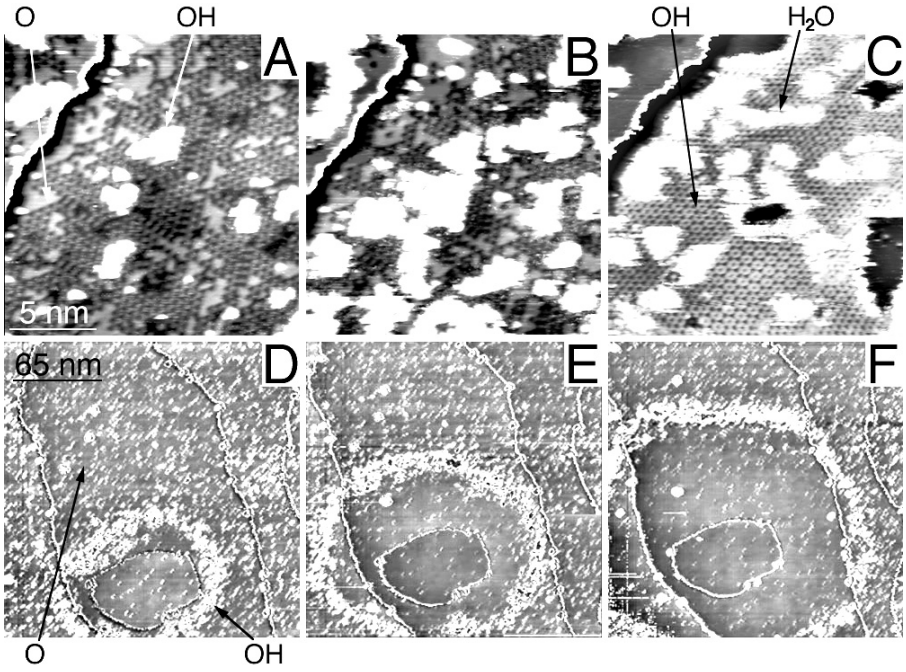

Fig. 1: (A) – (C): Series of successive STM images (17 x 17 nm^2) recorded during exposure of an O-covered Pt(111) surface at 112 K to 8 x 10^{-9} mbar H_2. The dark dots in (A) mark the O-adatoms in the initial 2 x 2-structure. The bright features are the growing OH_{ad}-patches. In (C) the area is mostly covered with ordered OH_{ad}-domains where the bright fuzzy patches covered by H_2O are developing.
(D) – (F): Larger scale (220 x 220 nm^2) images at 112 K and 2 x 10^{-8} mbar H_2. In (D) the bright dots are small OH islands which exhibit enhanced concentrations in a ring expanding into the O-rich region, leaving H_2O behind. (Thin lines are atomic steps.)

5.2.7.3 Overview of the Theoretical Background

Sets of coupled nonlinear ordinary differential equations (ODEs) of the type of Eq. (2) may be subject to systematic analysis of possible solutions in the framework of bifurcation theory [32, 33]. Bifurcation simply means a qualitative change of the dynamic behavior of a system upon variation of one of its control parameters, e.g., a transition from stationary to oscillatory behavior. The temporal behavior of a system described by two variables can only be stationary or harmonic oscillatory. These two situations are corresponding to fixed points or limit cycles, respectively, in a phase-space representation of the mutual dependencies of the two variables where time is eliminated. With three or even more variables the situation becomes much more complex and may involve so-called mixed-mode oscillations or chaotic behavior, the latter being characterized by "strange attractors" in the phase-space representation.

The specific nature of the differential equations describing the kinetics depends, of course, on the mechanism of the underlying elementary steps. However, it has been demonstrated that any exothermic reaction in an open system can give rise to bistable, excitable or oscillatory behavior for which the principle features may be obtained by using just a single unimolecular step [34, 35]. Various mathematical models have been proposed to describe oscillatory catalytic reactions, either as general models or adapted to specific experimental situations. The latter may quite often be traced back to one of the various types of general models which, e.g., may contain a slow buffer step [36], comprise coverage-dependent activation energies [37-41] or involve the creation of vacant sites [42, 43].

The decision as to whether a proposed scheme yields oscillatory solutions can, of course, be reached by integrating the differential equations or, even more elegantly, by applying a more general method denoted as stoichiometric network analysis (SNA) [44, 45].

As outlined in the introductory section, with any extended system the effects of spatial coupling between different parts play an important role. If coupling by diffusion is dominant, proper theoretical description has to be based on partial differential equations (PDEs) of the type of Eq. (3). The general nature of possible resulting concentration patterns has been explored quite extensively in connection with the analysis of chemical reactions in homogeneous solution [2, 5, 44–46]. The basic feature is that of a propagating "chemical" wave, as demonstrated by the experimental data of Fig. 1. Such waves were recognized already in 1906 [47]. They typically propagate with a velocity determined by $\sqrt{D \times k}$, where D is the diffusion coefficient and k an effective, first-order rate constant. Apart from propagating waves, stationary so-called Turing patterns [48] may be formed, with which phenomenon, for example, the periodic faceting of a Pt(110) surface in the course of CO oxidation was identified [49, 50].

The different types of chemical waves may be classified with regard to whether the medium is bistable, excitable, or oscillatory [2]. In a bistable medium a transition from one state to another (differing in concentration) may proceed via a propagating reaction front. In excitable media an external perturbation of sufficient strength may cause a transient excursion of the system to another state from where it returns to the initial state. After some refractory time it may then be excited again. Propagating pulses and spiral waves are the characteristic features of such a situation. In contrast, oscillatory media do not need external perturbation but perform autonomous periodic changes, associated, for example, with the formation of so-called target patterns, unless global coupling mechanisms are operating. Finally, irregular and rapidly changing patterns known as "chemical turbulence" may be formed, which represent the spatio-temporal counterpart of temporal chaotic behavior.

In a bistable system both states may coexist just at one specific value of the varied control parameter, while otherwise the less stable state is pushed away by a moving interface. If the front is not flat but exhibits a curvature with radius *R,* it propagates with a modified velocity $c = c_0 \pm D/R$ [2], where *D is* the diffusion coefficient and c_0 the velocity of the plane wave. Evidently a critical radius, $R = D/c_0$, exists below which $c < 0$, i.e., a front does not expand but shrinks. That means that R_C represents the critical radius for nucleation of a concentration wave in a defect region which is typically of the order of 1 μm, as determined for CO oxidation on Pt [51].

Spiral waves are ubiquitous in reaction-diffusion systems and characteristic for excitable media, whereby the excitation not necessarily requires an external perturbation, but quite frequently may be identified with an inherent local variation of kinetic parameters such as found with a defect zone on a surface. The general properties of spiral waves may be rationalized in the framework of the so-called kinematic approximation [2, 52, 53]. The core of a spiral on a catalytic surface is often formed by a defect, to which the spiral is 'pinned' and which determines its characteristic properties, such as rotation period and wavelength [52].

Global coupling is often decisive for the formation of patterns in oscillatory media. Depending on the kind of feedback, global coupling may either stabilize or destabilize the uniformly oscillating situation through symmetry breaking [54]. Systematic analysis of the kinds of pattern formation in an oscillatory medium with global coupling was performed with a model system, the modified Ginzburg-Landau equation, whose characteristic features are, however, of general validity [55]. It was shown that global coupling may, among others, modify or even suppress turbulent behavior.

With realistic systems, such as nonuniform surfaces, the observed spatio-temporal patterns may become quite complex due to superposition and coupling of differing contributions. Analysis may then become rather difficult. One is then interested in methods that allow extraction of the relevant features and simplification of the dynamics. A suitable technique is the Karhunen-Loeve decomposition into an optimal set of eigenfunctions, also known as proper orthogonal decomposition [56], which has already been successfully applied to catalytic reactions in a few cases [57, 58].

5.2.7.4 CO Oxidation on Pt(110): A Case Study of a Uniform Isothermal System

As mentioned above, kinetic oscillations associated with a catalytic reaction were first discovered with the oxidation of CO on supported platinum catalysts [6, 7], and it was also this reaction which was first investigated using the "surface science" approach, i.e., with well-defined single crystal surfaces under low pressure conditions [59]. It is still the system studied in most detail, among which the Pt(110) single crystal surface exhibits the richest variety of phenomena and is understood best.
The mechanism of this reaction is well established [60, 61] and proceeds schematically along the following steps:

$$CO + * \leftrightarrows CO_{ad}$$
$$O_2 + 2* \rightarrow 2\,O_{ad}$$
$$O_{ad} + CO_{ad} \rightarrow CO_2 + 2*$$

Here, * denotes a free adsorption site; this has a different meaning for the two adsorbates. Whereas dissociative oxygen adsorption is strongly inhibited by the presence of preadsorbed CO, the chemisorbed O atoms form

rather open adlayers, which do not significantly affect the additional uptake of CO (asymmetric inhibition). Under steady-state flow conditions the temperature has to be high enough (≥ 400 K) to enable continuous desorption of CO and creation of free adsorption sites, otherwise complete blocking of the surface by adsorbed CO would inhibit oxygen adsorption and, consequently, the catalytic surface reaction. Figure 2 shows the steady-state rate of CO_2 formation on a Pt(110) surface, which was either flat or periodically stepped (faceted), as a function of CO partial pressure, while the two other control parameters (p_{O_2} and T) were kept fixed. At low p_{CO}, the surface is largely covered by adsorbed oxygen, and the reaction rate is governed by the supply of CO and therefore rises proportionally to p_{CO}. Eventually, the stationary CO coverage becomes so high that it starts to inhibit oxygen adsorption noticeably, and further increase of p_{CO} causes a decrease of the reaction rate, which becomes now limited by oxygen adsorption. Since the faceted surface exhibits a higher oxygen sticking coefficient [62], for identical control parameters the rate also becomes larger. No such difference is observed at low p_{CO} where the rate is limited by CO adsorption whose sticking coefficient is not noticeably affected by the surface structure.

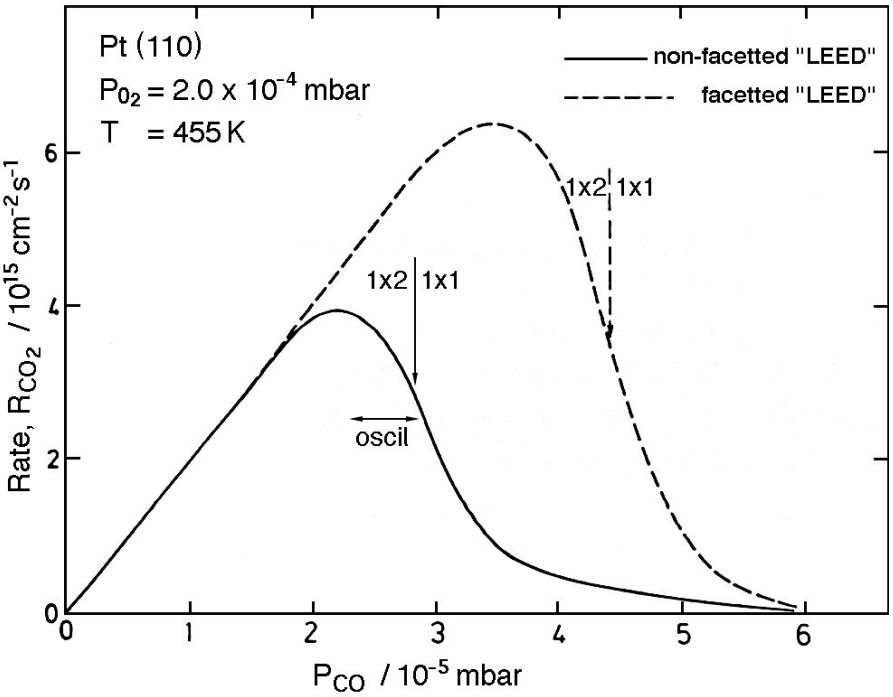

Fig. 2: Rate of CO_2 formation in catalytic CO oxidation at a Pt(110) surface, which is either flat (full line) or faceted (broken line) as a function of CO partial pressure p_{CO}, with the oxygen partial pressure p_{O_2} and temperature T kept fixed.

The steady-state kinetics can readily be modeled by solution of the corresponding differential equations for the CO and O coverages, and the resulting data may even be transferred to "real" catalyst systems [63]. The decrease of the rate with increasing p_{CO} becomes steeper at lower temperature (due to the increasing mean residence time of adsorbed CO on the surface), and the system eventually becomes bistable, exhibiting branches of high and low reactivity, and a clockwise hysteresis upon variation of p_{CO} [64, 65] which can readily be modeled with a two-variable system [66, 67]. While such a behavior is characteristic for the densely packed Pt(111) surface, novel effects – namely rate oscillations – come into play with the more open crystal planes such as (100) [59, 68], (110) [69] or (210) [70, 71].

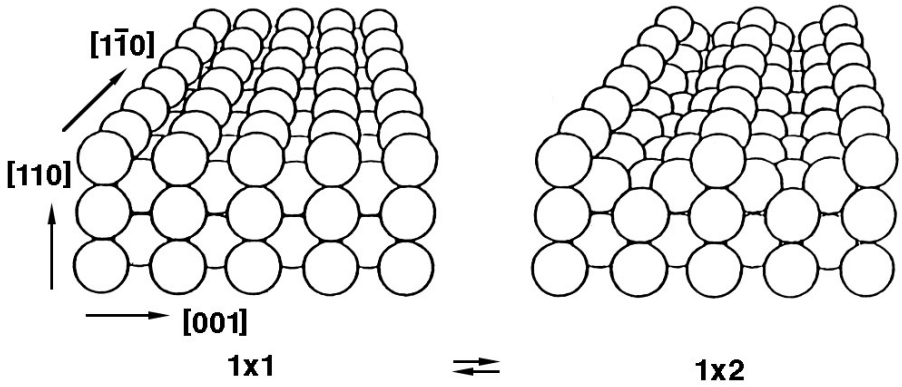

Fig. 3: The two structural modifications of the Pt(110) surface.

Returning to Pt(110), these oscillations occur within a relatively narrow range of p_{CO}, marked by a bar in Fig. 2, and are associated with a periodic variation of the atomic structure of the surface. As depicted in Fig. 3, the clean Pt(110) surface is reconstructed into a 1 × 2 "missing row" structure which is transformed into the normal 1 × 1 structure if the CO coverage exceeds a critical value of about θ_{CO} = 0.2 [72, 73]. This structural transformation is driven by the energetics of CO adsorption and is a rather local process, which involves displacements of surface Pt atoms only over short distances as demonstrated by scanning tunneling microscopy (STM) [74].

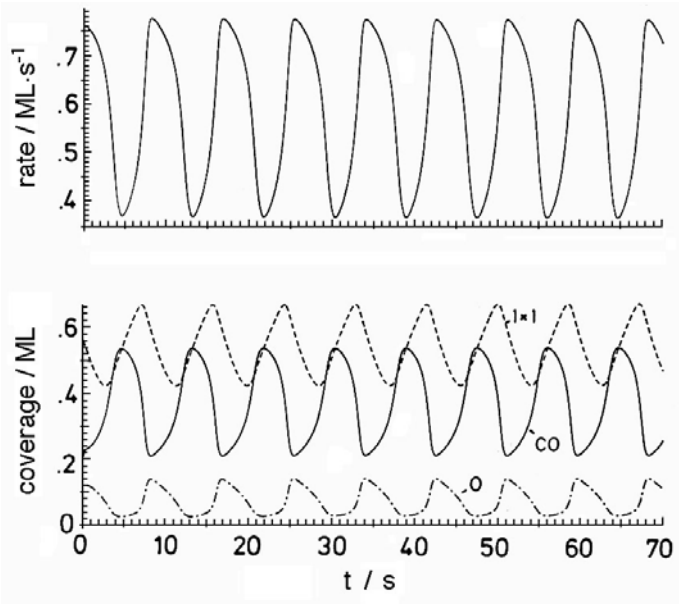

Fig. 4: Oscillatory behavior resulting from integration of the three ordinary differential equations modeling the kinetics of CO oxidation on a Pt(110) surface for a particular set of control parameters: T = 540 K, p_{O2} = 6.7 × 10^{-5} mbar, p_{CO} = 3.O × 10^{-5} mbar. Temporal variation of the reaction rate, the O- and CO coverages as well as the fraction of the surface being in the 1 × 1 structure, respectively (ML = monolayer) [66].

On the other hand, the oxygen sticking coefficient is larger on the 1 × 1 phase than on the 1 × 2 phase [74]. Since the kinetic oscillations are observed under conditions for which oxygen adsorption is rate-limiting, their occurrence may now readily be rationalized. Starting with the 1 × 2 surface, the p_{O2} : p_{CO} ratio will be such that sufficient CO is adsorbed to lift the reconstruction. On the 1 × 1 patches formed more oxygen will be adsorbed which then reacts with adsorbed CO, so that the coverage of the latter drops below the critical value for maintaining the 1 × 1 phase stable. The surface structure transforms back to 1 × 2 where the O_2 sticking coefficient is smaller, so that the

CO coverage may build up again, and so on. In this way, the microscopic surface structure acts as an atomic switch between states of high and low reactivity and is thus responsible for the occurrence of rate oscillations. Proper inclusion of the surface state as a further variable leads to a set of three ODEs, whose solutions exhibit, apart from steady-state, bistable, or excitable behavior, oscillatory kinetics for certain ranges of control parameters such as those displayed in Fig. 4 [66]. Note that the O and CO coverages are strictly anticorrelated, while the fraction of the surface being present as 1 × 1 phase oscillates with a phase shift and plays the role of a slow variable whose time constant is determined by the kinetics of the structural phase transition. The reaction rate strictly parallels the O coverage, and since the latter is reflected by the variation of the work function, $\Delta\varphi$, this quantity may serve as a convenient monitor for the rate oscillations rather than direct recording of the CO_2 partial pressure by means of a quadrupole mass spectrometer.

Figure 5 shows an experimental time series, which was recorded in this way, for which p_{O2} and T were kept strictly fixed, while p_{CO} was varied stepwise in small increments. (The onset of oscillations at even larger p_{CO} occurs via small amplitudes, which continuously grow upon decreasing the CO pressure as characteristic for a Hopf bifurcation [69].) The oscillations in Fig. 5 are at first strictly periodic, until at a certain value of p_{CO} (1.64×10^{-4} mbar) a qualitative change (i.e. bifurcation) occurs. Alternating small and large amplitudes are formed and the period is doubled.

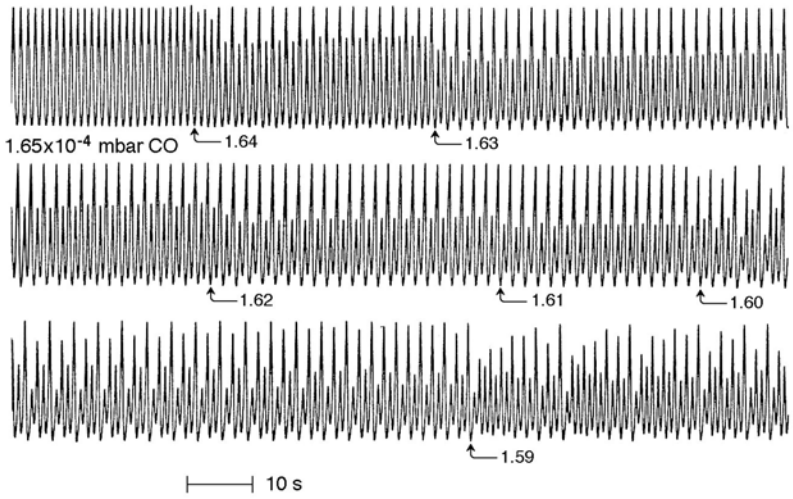

Fig. 5: Experimental time series of the rate of CO_2 formation on a Pt(110) surface: T = 550 K, p_{O2} = 4.0×10^{-4} mbar, the CO pressure was changed stepwise at the points marked.

Upon further decrease of p_{CO} the amplitude ratio continuously varies, until at 1.60×10^{-4} mbar another doubling of the period takes place. Further slight variation of p_{CO} to 1.59×10^{-4} mbar causes the appearance of irregular variations – a state known as deterministic chaos. The whole transition to chaos through the sequence of period doublings follows the well-known Feigenbaum scenario and is demonstrated more clearly by the phase portraits in Fig. 6, which were constructed from the corresponding time series [76]. Detailed analysis shows that for the chaotic state associated with a "strange attractor" one of the Lyapounov exponents became positive so that initially nearby trajectories in the phase space diverge. Analysis of another set of data recorded further inside the chaotic window revealed that then even two Lyapounov exponents became positive. This is a nice example for "hyperchaos" associated with a chemical reaction [77].

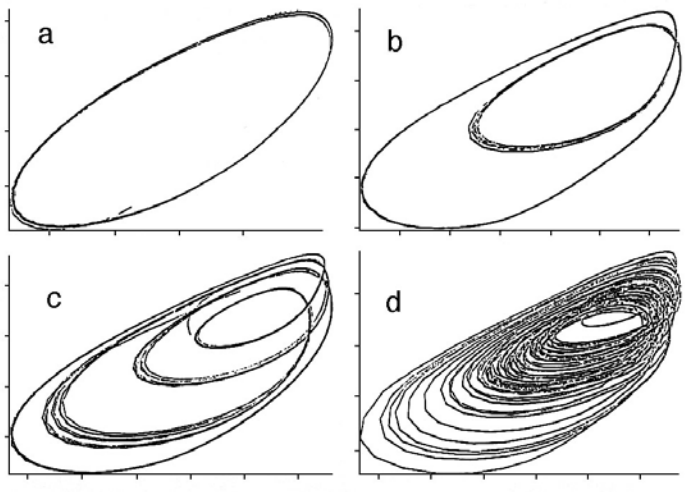

Fig. 6: Phase portraits constructed by the delay method from the experimental data of Fig. 5 for (a) $p_{CO} = 1.65 \times 10^{-4}$ mbar, (b) $p_{CO} = 1.63 \times 10^{-4}$ mbar, (c) $p_{CO} = 1.60 \times 10^{-4}$ mbar, and (d) $p_{CO} = 1.59 \times 10^{-4}$ mbar.

Although mathematical modeling, in terms of the quoted system of ordinary differential equations for the laterally uniform surface concentrations, accurately reproduces the stationary kinetics as well as the bifurcation to periodic (harmonic) oscillations, it fails to describe the period-doubling transition to temporal chaos [66]. This is because spatial coupling has been completely neglected; it was tacitly assumed that the whole macroscopic surface is always strongly synchronized, so that the concentrations depend only on time. As outlined above, this will generally not be the case, and as a consequence the formation of spatio-temporal concentration patterns is to be expected.

If nonisothermal effects are neglected, coupling by reaction-diffusion and global coupling through the gas phase have to be taken into consideration, and a proper theoretical description is achieved by inclusion of surface diffusion, so that the equations are extended into a set of partial differential equations (PDEs) of the type of Eq. (3) [51, 78, 79]. The resulting theoretical skeleton bifurcation diagram for the spatio-temporal pattern formation in the present system contains two excitable and an oscillatory region, as well as two bistable regimes with one- or two-front solutions.

Before discussing in some detail the characteristic features of these patterns, their experimental verification will be briefly described.

Imaging of lateral distributions of adsorbed species at low pressures was initially performed with scanning techniques [68, 80], which, however, suffer from limited spatial and temporal resolution. More recently, scanning photoelectron microscopy (SPEM) was employed to provide also chemical information with high lateral resolution [81, ´82]. Parallel imaging with also high temporal resolution is achieved by photoemission electron microscopy (PEEM) [83] which technique was used for recording of most of the images shown below. Related techniques such as low-energy electron microscopy (LEEM) and mirror electron microscopy (MEM) offer even higher lateral resolution but, have so far found only few applications [84-86]. Field emission and, in particular, field ion microscopy (FEM and FIM) [19, 20] enable almost atomic resolution to be achieved, but these techniques are confined to very fine tips (< 1 μm) where the extension of the individual crystal planes is far below the typical length scale of the reaction-diffusion patterns described.

The principle of PEEM is based on the differing dipole moments of adsorbate complexes, which give rise to modification of the local work function. The yield of photoelectrons emitted from a surface under the influence of ultraviolet irradiation is thus determined by the type and concentration of adsorbed species, and the lateral intensity distribution of these photoelectrons is imaged through a system of electrostatic lenses onto a channel plate and a fluorescent screen. From there, the PEEM images are recorded by means of a CCD (charge coupled device) camera and stored on videotape. Typical resolutions are 0.2 μm and 20 ms, respectively, the latter being determined by the video frequency. Since O atoms chemisorbed on Pt(110) cause a larger increase of the work function than adsorbed CO, regions predominantly covered by oxygen will appear dark in the images, while those on which CO prevails are grey.

Since the PEEM technique is based on the emission of electrons its application is restricted to the pressure range below about 10^{-4} mbar. In order also to observe pattern formation at elevated (up to atmospheric) pressures two optical methods were adopted: ellipsometry for surface imaging (EMSI) and reflection anisotropy microscopy (RAM) [88]. Both techniques are closely related and are based on recording images from light reflected from a surface. For EMSI the contrast is caused by local variations of the ellipsometric parameters, that is the complex refractive index and the effective 'thickness' of the surface layer (which is in the submonolayer range), while with RAM the contrast is based on different reflection anisotropy which again is sensitive to submonolayer coverages.

Even for those conditions under which the integral reaction rate is constant, the composition of the surface is not necessarily uniform, but may exhibit – frequently transient – propagating concentration patterns commonly known as chemical waves [16].

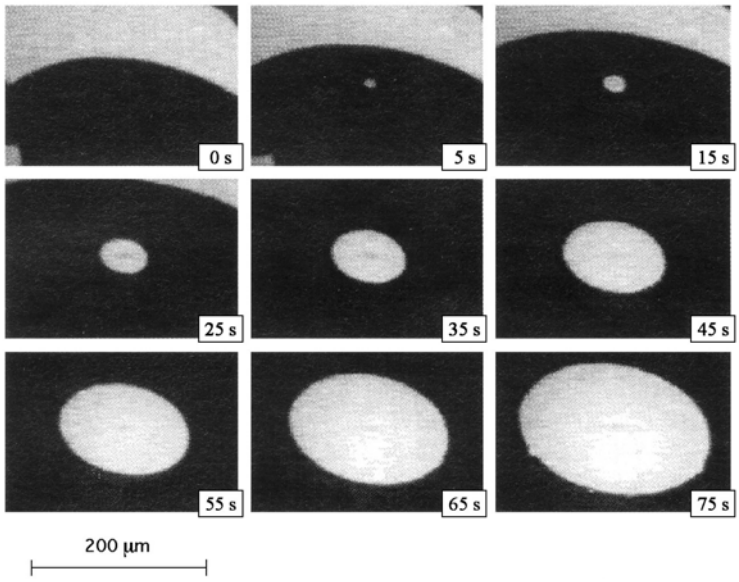

Fig. 7: Spatio-temporal concentration patterns on a Pt(110) surface during CO oxidation recorded by photoemission electron microscopy (PEEM) for conditions of dynamic bistability: $T = 443$ K, $p_{O_2} = 4 \times 10^{-4}$ mbar, $p_{CO} = 3.6 \times 10^{-4}$ mbar [89].

The CO + O_2/Pt(110) system exhibits, for example, parameter ranges in which both O and CO wave fronts are found to coexist and to propagate, as shown in Fig. 7 [89]. This situation is called "double metastability" or "dynamic bistability" and is also reproduced in model calculations [79]. The elliptical, rather than circular, shape of the growing islands is a consequence of the anisotropy of the diffusion coefficient for adsorbed CO, which is larger

along the (110) direction than along the perpendicular (001) direction [90]. The influence of the diffusion coefficient on the velocity of the front propagation is directly reflected by H/D isotope effects observed with the $O_2 + H_2$ and $NO + H_2$ reactions on Rh surfaces [91] as well as by "stop-and-go" effects at step bunches in the $CO + O_2$ reaction on Pt(100) [92]. As long as two consecutive fronts propagate with significantly different velocities, the faster eventually overruns the slower one. However, if the velocities become comparable, pulses with stable width are formed, which in a two-dimensional medium frequently develop into spirals.

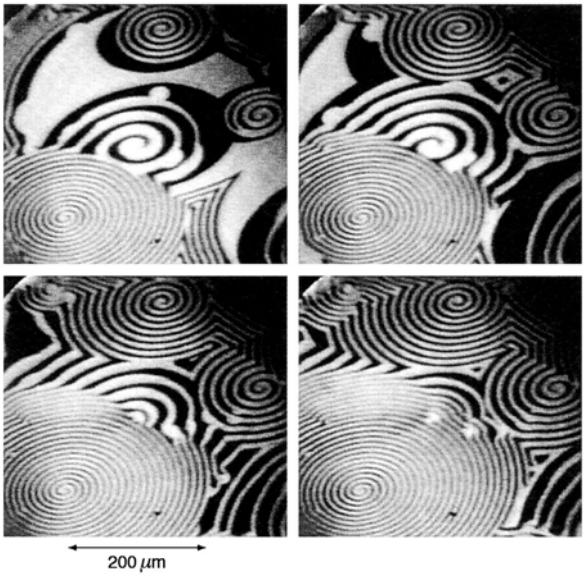

Fig. 8: PEEM images from a Pt(110) surface during CO oxidation exhibiting the not bold formation of spirals: interval between consecutive images 30 s, $T = 448$ K, $p_{O2} = 4 \times 10^{-4}$ mbar, $p_{CO} = 4.3 \times 10^{-5}$ mbar [89].

Such a situation is shown in Fig. 8. Remarkably, under identical external conditions, not all spirals exhibit the same periods and wavelengths, but rather continuous distributions. This has to be attributed to pinning of some of the spiral cores to surface defects of varying size and kinetic properties as reproduced by theoretical simulations [79]. Extended (≥ 10 μm) defects may even form the cores of multiarmed spirals [89].

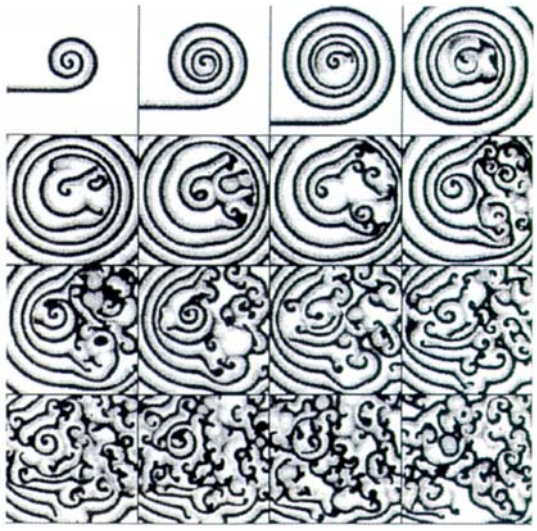

Fig. 9: Theoretical modeling of the temporal evolution of a turbulent state from spiral patterns [93].

Detailed theoretical modeling revealed that with the present system under certain conditions the spirals are migrating (meandering). Eventually, the Doppler effect becomes so pronounced that the spiral arms break up and cause a transition to irregular patterns such as shown in Fig. 9 [93] (chemical turbulence), quite similar to experimental observations (Fig. 10) [94].

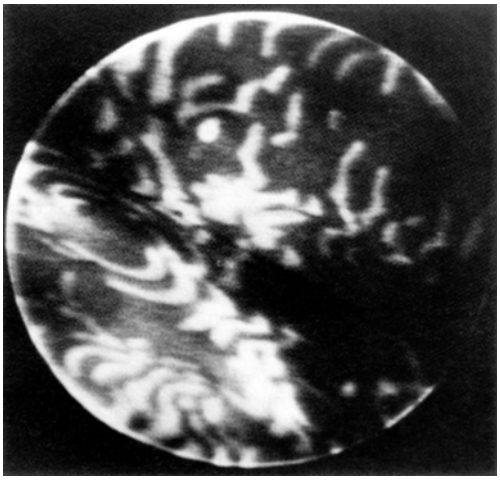

Fig. 10: Experimental verification of chemical turbulence with the CO oxidation at a Pt(110) surface [94]. Diameter of the PEEM image 0.5 mm.

The anisotropy of the surface diffusion with the present system also gives rise to a novel phenomenon, namely the formation of solitary pulses which propagate with constant velocity of about 3 μm/s along the (001) direction as reproduced in Fig. 11 [95]. Upon collision of two pulses these usually annihilate each other, as expected for reaction-diffusion systems, but sometimes one or even both pulses reemerged from the collision. The latter effect is denoted as soliton-like behavior. Moreover, occasionally a pulse was observed to emit another one in the opposite direction (wave splitting). Since the external parameters were identical everywhere, these unexpected effects have again to be attributed to the local defect structure of the surface. Under the assumption that the local $1 \times 1 \rightarrow 1 \times 2$ reconstruction is not perfect everywhere (and consequently the oxygen sticking coefficient also varies), all these phenomena could readily be reproduced by theory, as for example shown in Fig. 12 for the effects of soliton and wave splitting [96].

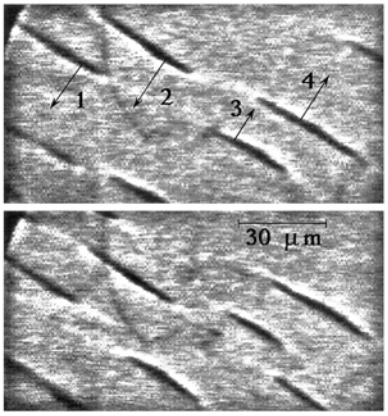

Fig. 11: Pathways for the reactions of benzene and oxygen molecule PEEM images, recorded at an interval of 3 s, from a Pt(110) surface during CO oxidation at $T = 485$ K, $p_{O2} = 3.5 \times 10^{-4}$ mbar, $p_{CO} = 1 \times 10^{-4}$ mbar. Dark pulses with increased oxygen coverage propagate as solitary waves along the (001) direction as indicated by arrows [95].

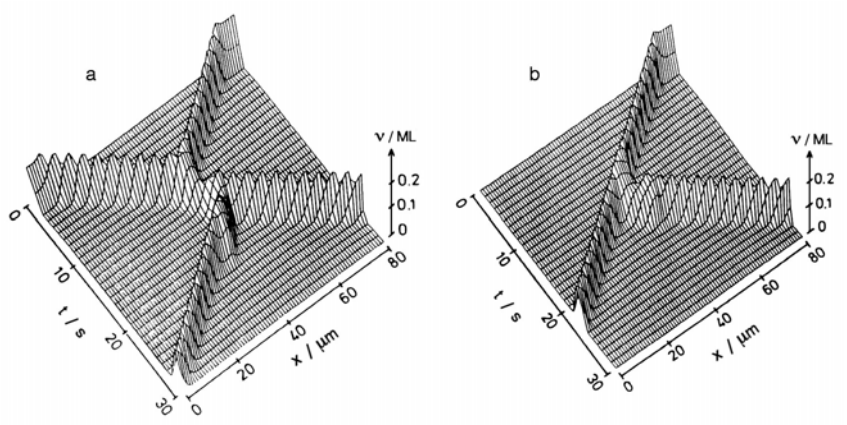

Fig. 12: Theoretical (one-dimensional) profiles of solitary waves propagating along the *x* direction with time where *v* denotes the concentration of O atoms causing the dark pulses in the PEEM images of Fig. 11: (a) collision of two pulses propagating in opposite directions in a defect region causes soliton-like behavior; (b) if a single pulse enters an appropriate defect zone, two pulses propagating in opposite directions are created (wave splitting) [96].

Parameter ranges, for which oscillations of the integral reaction rate occur, are characterized by global coupling of different parts via the gas phase [97], mainly by small variations of the CO pressure, since oxygen is present in large excess under oscillatory conditions. As a consequence of the asymmetric inhibition of adsorption, a slight decrease of p_{CO} (due to enhanced reactivity) increases the probability for oxygen adsorption and hence causes a positive feedback loop and favors synchronization. Frequently, the whole surface oscillates uniformly in phase. At lower temperatures (around 430 K) elliptical target patterns on an oscillatory background are also observed (Fig. 13) [94], which could be modeled theoretically by assuming defects acting as pacemakers [98]. At high temperatures (≥ 540 K), standing waves are also formed, which take the form of stripes of rhombic cells [94], which again could be modeled by taking gas-phase coupling into account [99], but for which complete theoretical description could be achieved only later by inclusion of the formation of subsurface oxygen [100]

In summary, the rich variety of phenomena associated with catalytic CO oxidation on Pt(110) single crystal surfaces under isothermal, low-pressure conditions has been widely explored experimentally and also understood theoretically.

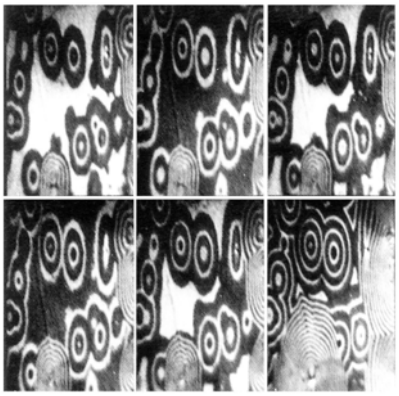

Fig. 13: A sequence of PEEM images (200 × 300 μm^2) recorded at intervals of 4.1 s (30 s between the last two images) from a Pt(110) surface during CO oxidation showing the evolution of so-called target patterns: T = 427 K, p_{O2} = 3.2 × 10^{-4} mbar, p_{CO} = 3.0 × 10^{-5} mbar [94].

5.2.7.5 Oxidation of Carbon Monoxide on Other Surfaces

Carbon monoxide oxidation has also been extensively studied with other catalysts. While the Langmuir-Hinshelwood reaction scheme formulated above is generally valid, there exist quite some differences both with respect to the observed phenomena as well as with the microscopic mechanisms causing kinetic instabilities.

Prior to Pt(110), the behavior of the Pt(100) single crystal surface was investigated in quite some detail [59, 68, 101-104]. Again, a reconstruction mechanism similar to that of Pt(110) is in operation. The clean Pt(100) surface exhibits a quasihexagonal (hex) configuration of surface atoms, which is transformed under the influence of adsorbed CO into the normal 1×1 configuration [105-109]. However, in contrast to Pt(110), there is now a much larger difference in the oxygen sticking coefficient, namely about 0.3 on the 1×1 phase and $< 10^{-3}$ on the hex surface [110, 111]. As a consequence, the parameter range for the occurrence of kinetic oscillations is much wider than with Pt(110) [97], and the global coupling mechanism through variations in the partial pressures is less efficient. This effect of imperfect lateral coupling causes the rate oscillations as well as the associated spatio-temporal concentration patterns to become much less regular than with Pt(l10). More recently a theoretical description based on an extended mean field approximation was presented [112].

Even on the Pt(110) surface the situation may become still more complicated. Under certain conditions, the structure of the flat surface transforms into a sequence of steps and terraces (facets), which process is associated with a continuous variation of the reactivity of the type as displayed in Fig. 2 [113]. In the absence of a catalytic reaction, thermally activated reordering takes place, and the initial situation is restored. The increase in reactivity has to be attributed to an enhancement of the oxygen sticking coefficient, as verified in experiments with a cylindrical Pt single crystal sample exhibiting all surface orientations of the (001) zone. There the (210) plane was found to exhibit the highest value of the O_2 sticking coefficient [114]. Indeed, the latter plane was also found to exhibit kinetic oscillations [70, 114]. Since the clean Pt(210) surface is not reconstructed, the simple reconstruction model at first seemed to fail to account for the oscillatory kinetics. However, it was found that this plane indeed facets under reaction conditions, preferably into (110) and (310) orientations. On the (110) (and related) microfacets then, the same mechanism is operating as with the respective extended single crystal surfaces [71]. Figure 14 displays an STM image from a Pt(210) surface after prolonged reaction where the facet formation is directly discernible [115]. Pattern formation on this type of facetted Pt(110) surfaces was explored in more detail by applying low energy electron microscopy (LEEM) with its improved lateral resolution [87].

Another, principally different mechanism comes into play, however, with CO oxidation on palladium at low pressures, and even occurs with Pt catalysts at higher pressures. Kinetic oscillations have been found with Pd(110) and (111) single crystal surfaces at total pressures exceeding about 10^{-3} mbar with a large excess of oxygen in the gas phase [116-119]. As outlined above, with Pt the normal Langmuir-Hinshelwood mechanism causes the appearance of a clockwise (cw) hysteresis in the CO_2 production rate, if the CO pressure is continuously increased and decreased again. With Pd such a cw hysteresis loop is also observed at low p_{O_2}, but it changes into counter-clockwise (ccw) upon increasing the O_2 pressure [117]. One therefore obtains a cross-shaped stability diagram by plotting the transition points of the cw/ccw hysteresis on a p_{O_2}/p_{CO} diagram [119], and the crossing point marks the lower limit of p_{O_2} for the occurrence of oscillations. This mechanism has to be attributed to the participation of another species, namely oxygen atoms which may be dissolved below the surface (i.e. subsurface oxygen)

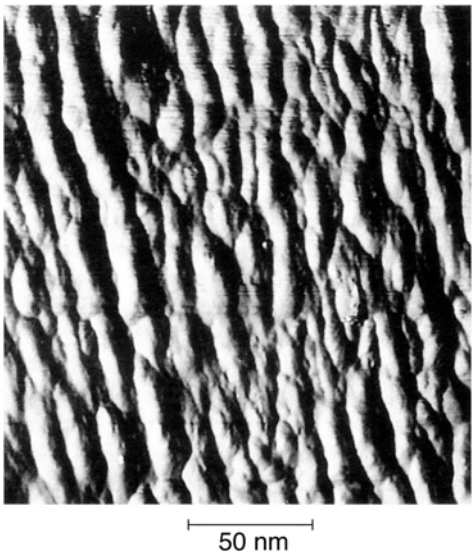

Fig. 14: Scanning tunneling microscopy (STM) from a Pt(210) surface after prolonged CO oxidation at T = 480 K, p_{O_2} = 2.0 × 10^{-4} mbar, p_{CO} = 6.7 × 10^{-5} mbar, demonstrating the formation of facets preferentially oriented along the (001) direction with average mutual spacings around 15 nm [115].

[117]. If the surface is largely covered with oxygen, O atoms will start to penetrate below the surface, whereby the surface itself becomes less active, i.e., the oxygen sticking coefficient is reduced. As a consequence, the surface becomes predominantly covered by CO, and now subsurface O atoms are segregating back to the surface from their reservoir until the initial situation is reestablished and one oscillation cycle is completed. Inclusion of such a subsurface species into the reaction model yielded satisfactory theoretical description of the observed kinetic phenomena [120, 121].

The existence of subsurface oxygen at Pd surfaces manifests itself mainly through the inverse dipole moment which leads to a lowering of the work function $\Delta\varphi$, instead of the increase usually caused by negatively charged O atoms *on* the surface [122, 123].

A similar subsurface species may also be formed on Pt(100) and (110) surfaces under low pressure conditions where the work function may become even lower (by up to 1 eV) than that of the clean surface which effect causes the appearance of very bright spots in the PEEM images [124, 125]. As outlined above, this species has to be included into the reconstruction model for a full description of the standing-wave patterns [100].

For platinum, the situation may also become quite different at higher oxygen pressures. It is known that for $p_{O_2} \geq 1$ mbar Pt may form oxides, and the timescale on which such oxides are reduced by CO, were found to be similar to the period of rate oscillations [126]. Therefore, an oxide model was proposed [127] which assumes that part of the active surface covered by chemisorbed oxygen atoms is transformed into an inactive oxide state. This oxide may then be slowly reduced by CO, whereby the initial active state of metallic Pt surface is restored. Experimental verification of this mechanism was sought in Fourier transform infrared spectroscopy (FTIR) experiments which were, however, not very conclusive [128, 129]. Indirect proof was obtained by solid-state potentiometry which experiments demonstrated that the conditions under which rate oscillations occur coincide with those for the formation of platinum oxides [130]. The application of in-situ X-ray diffraction with supported Pt catalysts revealed even more direct evidence for the operation of the oxide mechanism. From analysis of angular diffraction profiles it

was concluded that the rate oscillations are associated with periodic oxidation and reduction of PtO and Pt_3O_4, reaching a maximum degree of oxidation of about 20–30% [131]. It is felt that the oxide mechanism is prevailing in CO oxidation on Pt catalysts, whenever the experiments are performed near atmospheric pressure, even if single crystal samples are used [132]. Theoretical modeling of the transition to oxide and its influence on the kinetics of CO oxidation shows good agreement with experimental observations [133].

Still another mechanism, the carbon model, was proposed in order to explain kinetic instabilities in CO oxidation [134, 135] in which it was assumed that deactivation of the surface by buildup of C atoms is followed by their oxidative removal. So far, however, no convincing evidence for the operation of this mechanism can be offered.

It should be mentioned in this context, that with CO oxidation on polycrystalline Pt catalysts near atmospheric pressure conditions, not only more or less regular periodic rate oscillations were found, but that chaotic temporal behavior was also identified in a number of studies [136-139].

5.2.7.6 Other Isothermal Systems with Oscillatory Kinetics

Apart from CO oxidation, quite a number of other catalytic systems was found to exhibit rate oscillations and other kinetic instabilities which have not primarily to be attributed to thermokinetic effects but to the underlying surface chemistry. Among these, reactions of NO with either CO, H_2, or NH_3 on a Pt(l00) single crystal surface have been explored in most detail and will hence be described here to some extent. These reactions have a basic feature in common, namely an autocatalytic step associated with the dissociation of adsorbed NO.

With the reaction $NO + CO \rightarrow \frac{1}{2} N_2 + CO$, kinetic oscillations were observed with a polycrystalline Pt ribbon in the 10^{-4} mbar pressure range [140], following a short report on such effects with Pt(100) at extremely low pressures ($\approx 10^{-9}$ mbar) [141]. Subsequently, this reaction became subject of extended investigations with Pt(100) in the 10^{-7} to 10^{-5} mbar pressure regime [142–148]. No oscillations were observed on Pt(111) and Pt(110), which planes were found to be much less reactive in dissociating NO, in accordance with findings made with the cylindrical Pt single crystal sample [146]. With Pt(100) kinetic oscillations occur over a wide range of the $p_{NO} : p_{CO}$ ratio within two temperature windows. In the low temperature ($\leq$ 430 K) range the oscillations occur on a pure 1×1 substrate. They are not sustained but may be initiated by a small temperature jump after which they decay within a few cycles [144]. This effect is due to insufficient lateral coupling as was verified by imaging spatio-temporal concentration patterns by PEEM [148]. Periodic modulation of the temperature with small amplitude ($\approx$ 1-3 K) suffices to create sustained oscillations [145]. In the upper temperature range ($\geq$ 450 K) the oscillations are not damped and occur on a laterally uniform surface, whose structure switches periodically between 1×1 and hex, similar to the CO oxidation reaction. The transitions to steady-state rates at both limits of the high temperature range are illustrated by the bifurcation diagram reproduced in Fig. 15. At the upper limit, oscillations develop via a Feigenbaum scenario from small amplitude chaotic oscillations, while at the lower limit the transition to stationary kinetics is discontinuous and associated with the onset of spatio-temporal pattern formation [147, 148].

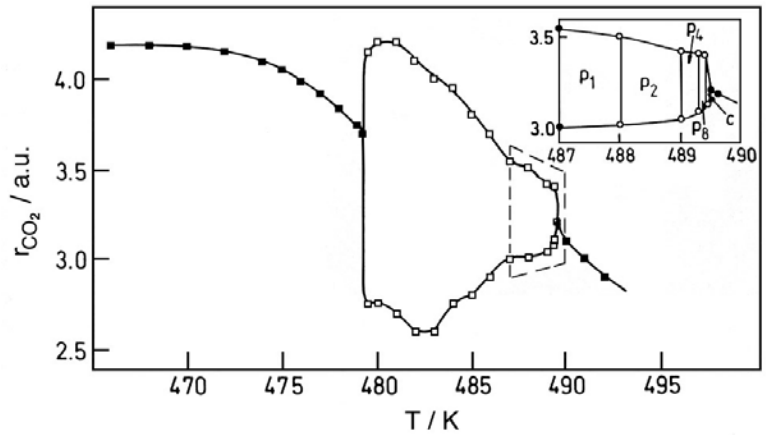

Fig. 15: Bifurcation diagram for the NO + CO reaction on Pt(l00) for fixed $p_{CO} = p_{NO} = 4 \times 10^{-6}$ mbar as a function of temperature T in the upper temperature window. Open squares denote the amplitudes in the oscillatory regime, while full squares represent stationary rates. The inset shows the Feigenbaum scenario with the sequence of period doublings (p_1 to p_8) and transition to chaos (c) [147].

The mechanism of the NO + CO reaction (with formation of N_2O in a side reaction being neglected) involves dissociation of adsorbed NO as rate-limiting step [144]. This process, $NO_{ad} + * \rightarrow N_{ad} + O_{ad}$, requires (formally) an additional vacant adsorption site (*). In the subsequent steps of product formation, namely $2\ N_{ad} \rightarrow N_2 + 2*$ and $CO_{ad} + O_{ad} \rightarrow CO_2 + 2*$, more free sites are created than are consumed by the initiating process of NO dissociation. Hence, autocatalysis with respect to the formation of free sites is the consequence, which explains the occurrence of a surface explosion, i.e., of extremely narrow peaks, in thermal desorption spectroscopy experiments with NO + CO coadsorbed on Pt(100) [149, 150]. This autocatalytic process is also responsible for the occurrence of kinetic oscillations without involving a structural transformation of the surface as demonstrated by proper theoretical modeling [144, 151]. It therefore accounts for the experimental observations in the low-temperature window.

The oscillations in the high-temperature range are associated with the adsorbate-driven hex 1×1 transformation of the surface structure. A qualitative theoretical description could be achieved by including this step in the model [144], which was recently extended further by incorporating more accurately the growth kinetics of the 1×1 phase triggered by lifting the hex reconstruction [152]. Even then, however, the agreement between theory and experiment is not completely satisfactory, most probably due to the presence of surface defects which play a significant role in the dissociation of NO [144] and may be modified by the reaction [153]. Recent Monte Carlo simulations based on the model of NO dissociation at the domain boundaries provide, however, good qualitative agreement with experiment [154].

Reduction of NO by either H_2 or NH_3 does not proceed along single pathways but through branching channels whereby the aspect of selectivity also comes into play. In the NO + H_2 reaction on Pt(100) both N_2 and NH_3 are formed (apart from a minor yield of N_2O) [155, 156] whereby chaotic kinetics were also identified [157].

This reaction was more extensively studied more recently with various Pt-group single crystal surfaces [158-161] as well as with the small facets imaged in field ion microscopy (FIM) [162-164]. These experimental studies were complemented by theoretical modeling and analysis [165-168]. In the NO + NH_3 reaction the main products are N_2 and N_2O, and oscillatory kinetics were found both with polycrystalline platinum at higher pressures [169, 170] as well as in the 10^{-7} to 10^{-5} mbar pressure range with Pt(100) [171, 172]. The dynamic behavior of both systems is nearly identical, and the mechanism is obviously rather similar to that in the NO + CO reaction. Conse-

quently, successful mathematical modeling could be achieved on the basis of an analogous reaction scheme [173], and the participation of the hex ⇆ 1 × 1 structural transformation was demonstrated experimentally [171, 174].

NO is much more readily dissociated on Rh than on Pt, and oscillatory kinetics with this catalyst material were again found with the NO + H_2 and NO + NH_3 reactions with field electron microscopy [19, 175] as well as with a Rh(110) single crystal surface [176]. In the latter study, by applying PEEM, quite unusual spatio-temporal patterns of the type shown in Fig. 16 were detected, namely rectangularly shaped target patterns and spiral waves. This effect has been attributed to an anisotropy of the surface diffusion, which, in addition, is influenced by adsorbate-induced reconstruction effects [177].

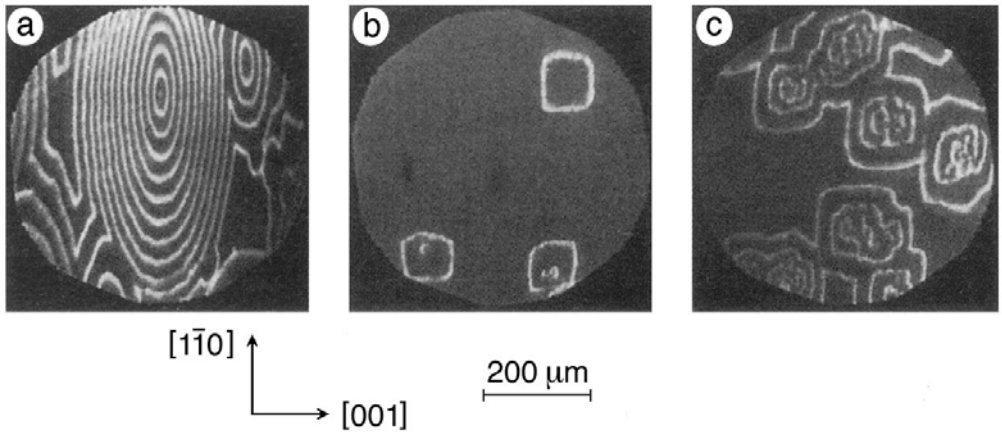

Fig. 16: Concentration patterns associated with the NO + H_2 reaction on a Rh(110) surface: (a) elliptical target patterns, T = 427 K, p_{NO} = 1.6 × 10^{-6} mbar, p_{H_2} = 1.8 × 10^{-5} mbar; (b) nucleation of square-shaped target patterns, T = 595 K, p_{NO} = 1.6 × 10^{-6} mbar, p_{H2} = 5 × 10^{-5} mbar; (c) same conditions as (b) but 60 s later [176].

The H_2 + O_2 reaction on Pt deserves brief mentioning in this connection. The propagation of concentration waves starting from the elementary steps on atomic scale was already discussed in sect. 5.2.7.2 in order to illustrate the formation of spatio-temporal patterns on mesoscopic scale. Under steady-state flow conditions kinetic oscillations at high pressures had been reported quite early for this system [9] and were later investigated again in quite some detail [178]. More recently, the heat generated with this reaction at a pressure of 10^{-2} mbar was directly determined experimentally [179]. Obviously, the quoted studies were not conducted under isothermal conditions so that heat transfer comes into play which effect does, however, not account for the observed time scales of oscillations. Nevertheless, the experimental findings could be satisfactorily modeled on the basis of an oxidation-reduction mechanism similar to that proposed for CO oxidation [180]. However, the correct mechanism has to include the autocatalytic step O + H_2O → 2OH as outlined above.

No kinetic oscillations could be observed with this reaction on an extended Pt(100) single crystal surface at low pressures, but merely simple bistable behavior. Interestingly, if a field emitter tip was used instead, on which the (100) plane of only about 50 nm diameter was adjacent to other crystal planes, oscillatory phenomena occurred [181]. It is felt that this effect is of more general relevance for the catalytic properties of small particles and it is therefore discussed further below.

5.2 7.7 Thermokinetics

Due to the pronounced temperature dependence of chemical rate processes, even small deviations from isothermal conditions are expected to be of strong influence on the dynamic behavior. Such effects are very likely to occur in any studies with "real" (either monolithic or supported) catalysts conducted near atmospheric pressure, where frequently temperature changes of several tens of degrees or even more are found.

Local variations of temperature can most conveniently be recorded by infrared thermography [182], and numerous reports on such phenomena associated with catalytic CO oxidation on supported catalysts can be found in the literature [183–188]. Among others, these experiments demonstrated the importance of thermal coupling between different catalyst pellets, whose variation affects the degree of synchronization of the rate oscillations [187, 188]. By using a thin evaporated Pt film, the propagation of reaction waves during CO oxidation could be studied [189]. In another experiment with the same reaction, a Pt wire was used which was solely heated by the enthalpy released by the reaction. It turned out that the oscillatory behavior changed substantially if the wire loop was cut into two parts, again demonstrating the importance of heat transport in such systems [190].

Coupling of chemical rate oscillations to temperature variations and then in turn of periodic deformation of a thin (200 nm thick) Pt(110) single crystal surface was recently demonstrated with the CO oxidation [191] as shown by Figure 17. As sketched in part A, the thin sample of about 4 mm diameter was placed across a hole of a bulk Pt sample. Kinetic oscillations with a period of ~5 s established at a 5 x 10^{-3} mbar O_2 partial pressure caused temperature variations of the central part by about 30 K which in turn caused periodic deformations reproduced in (B) as measured by integrating the reflected light intensity from the square marked in the third frame of (C). Part C shows diffuse light images from the catalyst's surface deformations at the 4 instants marked by dots in (B). Detailed mathematical analysis of the interplay between chemical reaction, heat evolution and mechanical deformation provided profound rationalization of the mechanism underlying these 'heartbeats of a catalyst'.

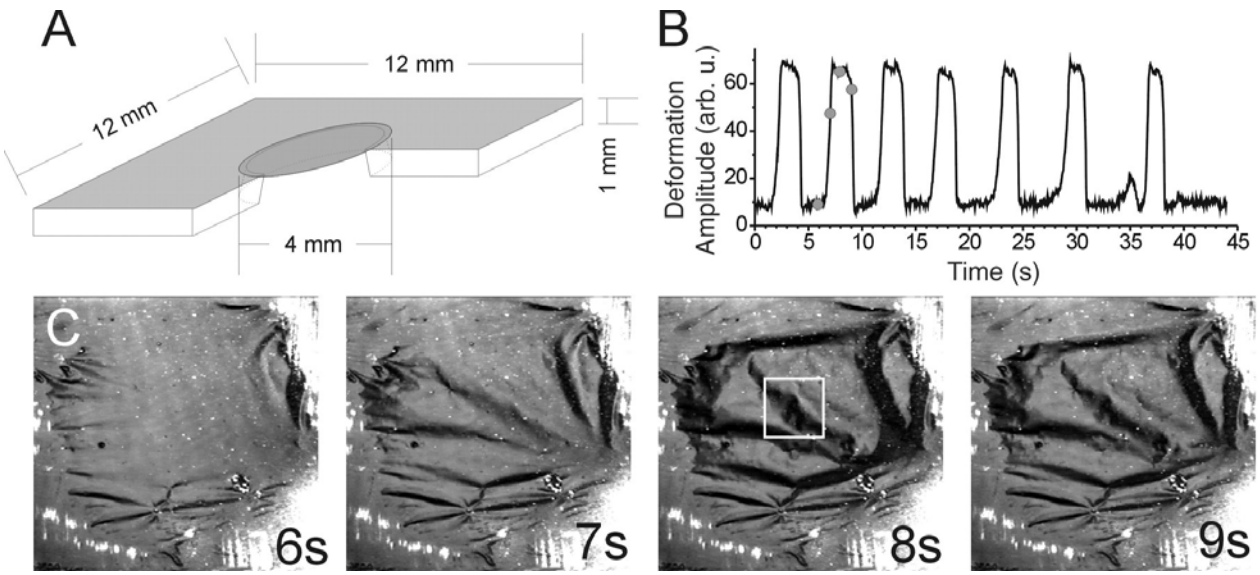

Fig. 17: Thermomechanical instability of a thin (200 nm) Pt catalyst during oscillatory CO oxidation [191].
(A) Catalyst and substrate geometry
(B) Deformation amplitude as a function of time
(C) Images (4.4 x 4.4 mm^2) from the catalyst deformation at the instants marked by dots on (B).

Systematic studies on wave propagation in electrically heated wires have been reported for various reactions, including oxidation of ammonia and hydrocarbons [182, 192–198] as well as the endothermic decomposition of CH_3NH_2 on a Pt wire [199]. Stationary (Turing) patterns as well as moving fronts were observed, the latter being associated with macroscopic rate oscillations. As an example, Fig. 18 shows the irregular motion of fronts associated with oxidation of propene on a Pt ribbon which was heated electrically and maintained at constant total resistance, whereby the integral kinetics became chaotic (Fig. 19) [196].

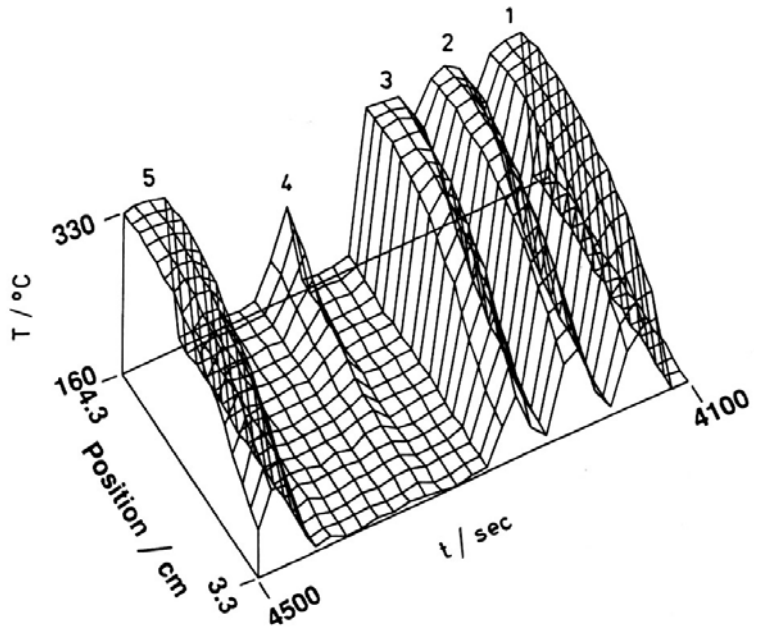

Fig. 18: Space-time diagram of the temperature profile of a 1 cm long segment of a Pt ribbon during oxidation of propene. While the average temperature is kept constant, a local temperature front moves back and forth [196].

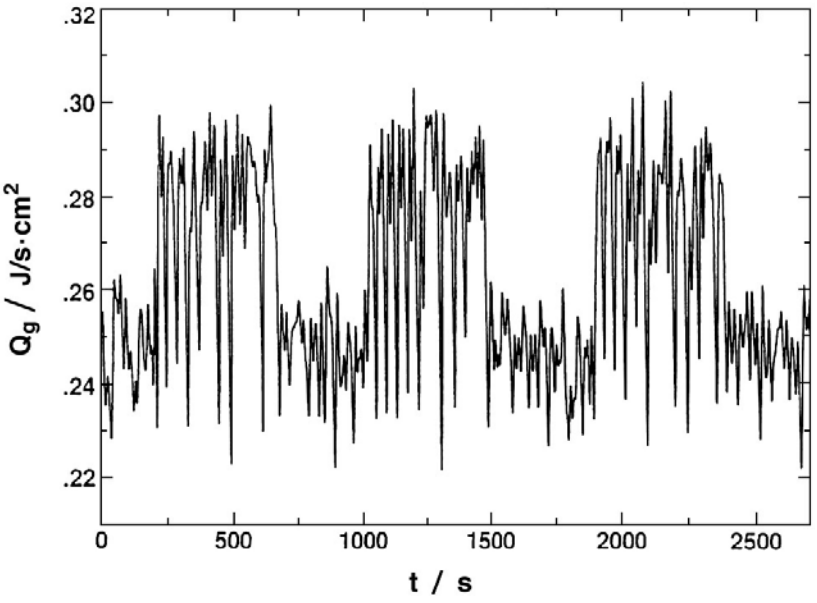

Fig. 19: Chaotic oscillations of the total heat generated by propene oxidation on an electrically heated platinum ribbon while the electrical resistance is kept constant [196].

Instead of keeping the resistance (= average temperature) constant, similar experiments were performed under different constraints, in which either the voltage or the heating current [195] was kept constant, and the resulting dynamic properties were found to differ significantly. Quite generally, such conditions represent global constraints and may lead to spatio-temporal pattern formation as a consequence of symmetry breaking [200, 201].

However, similar types of patterns may also be formed without external constraints, such as those observed with the oxidation of hydrogen on a Ni ring without additional electrical heating [202, 203]. Under certain conditions, a pulse rotating around the Ni ring with a period of about 10 min was observed. The integral behavior exhibited oscillations with three maxima and minima per rotation period. This effect demonstrates that the rotating pulse changes its shape periodically which is most likely due to nonuniformities of the catalyst.

If two-dimensional (e.g. foils) rather than one-dimensional (rings or wires) catalysts are used, the resulting spatio-temporal patterns are usually still more complex, as demonstrated with the $H_2 + O_2$ reaction on Pt [204, 205] and Ni [194, 206].

Various approaches can be found in the literature to implement nonisothermal effects in the theoretical modeling of the (integral) kinetics. For example, a simple mechanism for thermokinetic oscillations is possible in which catalytic sites are blocked at low temperature and reactivated at higher temperature. Such schemes have been analyzed in general form [207, 208] and applied to various oscillatory reactions such as NO + CO on Pd [209], $H_2 + O_2$ on Pt [64] and, in particular, $CO + O_2$ on Pt [210–212] as well as with the endothermic decomposition of CH_3NH_2 mentioned above [199]. The basic mechanism of the kinetic oscillations in this latter system (exhibiting temperature amplitudes of up to 500 K) is in fact rather simple. In the reactive state the temperature drops due to the endothermicity, and at low enough temperature the surface is then blocked by an inhibiting species. As a consequence, the continuing electrical heating causes the temperature to rise again, until the inhibiting species desorbs and the high reactivity is restored.

Although with most of the systems discussed in this section the details of the reaction mechanism and of the kinetics of the elementary steps is much less understood than for the well-defined single crystal systems described in the preceding sections, in these cases the basic features of spatio-temporal pattern formation could also be modeled successfully. This is because the decisive effects are thermokinetic in nature and can be approximated by a heat-balance equation in which the chemistry of the reaction is reduced to a single variable and the surface diffusion of the adsorbates is neglected [213–218]. Coupling through the gas phase may also be mostly neglected, although its inclusion may give rise to quantitative changes [213]. The basic equations take the general (dimensionless) form

$$\varepsilon\frac{\partial T}{\partial t} - \frac{\partial^2 T}{\partial x^2} = f(T,\theta,I) = Q_R - Q_{Ex}\left[+ Q_H(I)\right] \qquad (4)$$

$$\frac{d\theta}{dt} = g(\theta,T). \qquad (5)$$

The term $f(T, \theta, I)$ denotes the heat balance, Q_R is the heat generated by the reaction, Q_{Ex} is the heat exchange with the surroundings, and $Q_H(I)$ is the energy input by electric current I, if applied. The term $g(\theta, T)$ repre-

sents the surface chemistry of the catalytic reaction, with θ being a characteristic concentration variable. Typically, a species with concentration θ is consumed by the decisive reaction step and is produced in another process.

Various types of solutions were extensively discussed in the quoted literature. It is just mentioned that for certain parameter ranges many stable solutions were found to coexist, depending on the initial conditions. That means that even for identical steady-state control parameters the dynamic behavior may differ considerably, which renders this field rather complex.

5.2.7.8 Composite Surfaces

Modification of the activity of a catalyst surface by uniform distribution of foreign atoms is common practice. A prominent role is played by alkali metals which frequently act as promoters. Apart from their local effect, however also phenomena on mesoscopic scale may come into play with systems exhibiting characteristics of spatio-temporal self-organization as observed in studies with the O_2 + H_2 reaction on a Rh(110) surface [219, 220]. Depending on the reaction conditions, potassium condenses reversibly into mesoscopic (>1 □m) islands where it is coadsorbed with O and becomes also subject to mass transport with the reaction fronts. Differences in the mobility and the bonding strength of K on the O-rich and the reduced surface regions are the key factors for the formation of these concentration patterns.

Also immobile foreign atoms may alter the kinetic properties of a surface beyond the atomic scale. In the case of CO oxidation on Pt(110) [221] or Pt(100) [222] surfaces covered by submonolayers of Au atoms the presence of the gold atoms reduces the adsorption probability for oxygen and the diffusion coefficient for adsorbed CO if averaged over mesoscopic length scales, causing alterations of the velocities for the propagation of O- and CO-waves.

Fig. 20: PEEM image from a Pt(110) surface on which the left part was covered by 5% of a monolayer of Au during CO oxidation: T = 460 K, $p_{O2} = 4 \times 10^{-4}$ mbar, $p_{CO} = 4.6 \times 10^{-5}$ mbar [230].

Fig. 20 shows a PEEM image from a Pt(110) surface during steady-state CO oxidation where a part of the surface was uniformly covered by about 5% of a monolayer of Au atoms, while the other part was pure platinum. Both the phenomenology as well as the dynamics (velocity of wave propagation) of the patterns are obviously significantly affected. At the boundaries between domains with different Au content propagating straight fronts exhibit phenomena of refraction and reflection as in optics.

Instead of modifying a catalytic surface homogeneously, e.g. by uniform deposition of another material, as a next step heterogeneous structures with appropriate dimensions may be fabricated. It is known that formation and propagation of nonlinear waves may be markedly affected by the spatial boundary conditions in that, for example, certain modes are selected, or the motion through narrow channels is suppressed etc. [223–225]. Photolithographic techniques, as developed for microelectronics, offer a convenient way to prepare surfaces with such microstructures. The first experiments of this type were performed with a Pt(110) surface, onto which a titanium mask was deposited. The latter material oxidizes and is then completely inert in the CO oxidation reaction which is hence restricted to the bare Pt areas [226]. A PEEM image from such a surface exhibiting the propagation of concentration patterns is reproduced in Fig. 21. In the meantime, this approach has been extended to other systems, including microdesigned surfaces with more than one active component [227-234] and demonstrating the richness of phenomena to be observed. As an example, Fig. 22 shows PEEM images from a microstructured Rh/Pt(100) surface in the course of the NO + H_2 reaction [229].

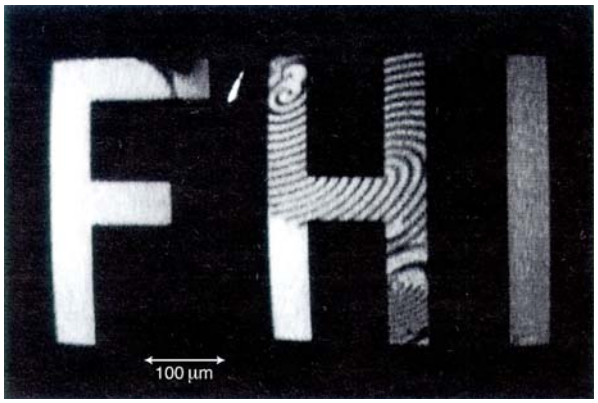

Fig: 21: Pattern formation on a microstructured Pt(110) surface during CO oxidation. Two of the patches are in uniform states while on the letter H spirals and propagating pulses develop [226].

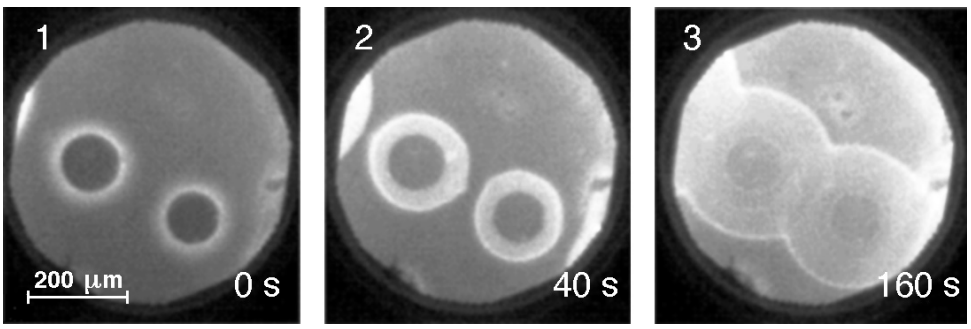

Fig. 22: PEEM images from a microstructured Pt(100)/Rh surface during the NO + H_2 reaction at p_{NO} = 2 x 10^{-6} mbar, T = 473 K. The reaction was initiated by rising the H_2 pressure from 2 x 10^{-6} to 7 x 10^{-6} mbar. Reaction fronts nucleate at the perimeters of the Pt islands (dark circles) and propagate into unreactive O-covered state on Rh.

5.2.7.9 Microscopic Scale Processes

The small particles of a "real" supported catalyst usually have dimensions of only a few nm**,** much smaller than the typical patterns found with isothermal reaction-diffusion systems on extended uniform surfaces. Typical nonlinear effects with such systems are therefore usually of thermokinetic origin, for which only the properties averaged over macroscopic (≈ 1 mm) length scale are of significance, as outlined above.

Quite different problems come into play, however, if processes occurring near the atomic scale become subject of closer inspection. On the theoretical side, formulation of kinetics in the framework of a mean-field description in terms of differential equations becomes questionable. Such an approximation is per se only justified if the mobility of the adparticles is sufficiently high and if interactions between them may be neglected. An alternative approach consists of performing lattice-gas-type computer simulations [235], among which models for CO oxidation have attracted particular attention [236–238].

The experimental situation has been significantly affected by the possibility of observing nonlinear phenomena with near-atomic resolution by the application of field emission and field ion microscopic techniques (FEM and FIM) as outlined above. Even if well-developed patterns such as spirals may not develop for geometric reasons on the small tips used in these experiments, propagating reaction-diffusion waves may become clearly discernible. Usually, their interfaces are much sharper than expected for reaction-diffusion systems of noninteracting particles, and this effect is most likely attributed to the operation of attractive interactions by which mean-field descriptions become invalid, and which may indeed lead to the formation of very sharp interfaces and even to "uphill" diffusion opposite to an existing concentration gradient [239].

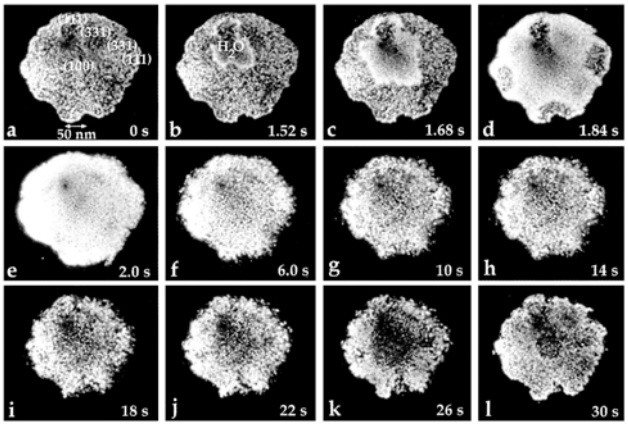

Fig. 23: Series of field ion microscopy (FIM) images from a Pt tip during the $H_2 + O_2$ reaction at 300 K : $p_{H2} = 6 \times 10^{-4}$ mbar, $p_{O2} = 5 \times 10^{-4}$ mbar. Imaging gases are O_2 and H_2O formed by the reaction [181].

A quite interesting effect was observed with the $H_2 + O_2$ reaction on Pt [181]. As outlined above, on an extended Pt(100) surface only bistable behavior is found, whereas if the same plane is exposed as small area on a field emitter tip under certain conditions oscillatory behavior is observed. This is illustrated by the sequence of images reproduced in Fig. 23. The central Pt(100) region becomes periodically activated by reaction-diffusion waves triggered from adjacent higher index planes, and as a consequence also the time-averaged reactivity of this plane is much higher than if existing isolated. It is important to distinguish this effect from the phenomenon of "spillover",

well-known in catalysis which is just due to *diffusion* of reacting species from one part of the surface to the other [206]. In the present case, it is the *coupling of reaction and diffusion*, which causes the propagation of nonlinear concentration waves under conditions far from equilibrium and thus affects the overall reactivity.

It is felt that such phenomena are of general importance for the reactive properties of small supported catalyst particles whose dimensions are comparable to those of a field emitter tip. Their activity is commonly considered to be simply composed by a superposition of the contributions from the different crystal planes and other structural elements such as steps and edges.

Extended computer simulations for models representing small catalyst particles demonstrated the limitations of this linear approach and the significance of sketched nonlinear effects [241– 245]. On the experimental side it was recently demonstrated that macroscopically observed bistabilities are drastically affected by particle size which effect was attributed to coverage fluctuations influencing the kinetics on small catalyst particles [246].

5.2.7.10 Controlling the Kinetics

So far the nonlinear phenomena were discussed under the conditions of steady-state of the external parameters (p_j, T), but their variation may give rise to novel effects.

Periodic variation of the reactant partial pressure p_j on catalytic conversion in real systems has already been extensively studied [247-254]. In the case of a system exhibiting already autonomous rate oscillations (under steady-state flow conditions) with period T_o the response to external forcing with period T_{ex} and amplitude A may be classified in the following way [255-257]: If the resulting period of the system T_r exhibits a fixed phase relation to that of the modulation T_{ex}, the system is entrained, and the ratio T_r/T_{ex} may be expressed as that between two small numbers k/l. For k/l = 1 the entrainment is called harmonic, for k/l >1 superharmonic, and for k/l < 1 subharmonic. If the phase difference between response and modulation is continuously varying, the oscillations are denoted as quasiperiodic. The characteristics of such a system may be rationalized by a “dynamic phase diagram”, in which regions of entrainment and quasiperiodicity are marked as a function of T_{ex}/T_o and A. The structure of such a diagram does not depend on the specific features of the reacting system, but only on its type of bifurcation around which the perturbation is applied [256, 257].

Single crystal experiments with periodic modulation of partial pressure have been performed with CO oxidation on Pt(100) [258] and Pt(110) surfaces [22]. Fig. 24 shows a sequence of time series for entrained and quasiperiodic oscillations for the latter system. The resulting experimental phase diagram (Fig. 25) is in good agreement with the results of a theoretical treatment based on the mechanism sketched above [259].

The formation of spatio-temporal concentration patterns associated with periodic forcing of the CO oxidation on Pt(110) via the CO partial pressure was investigated in detail more recently [260]. Near harmonic entrainment intermittent turbulence characterized by the formation of localized turbulent bubbles on a homogeneously oscillating background and disordered cellular structures are observed, while for the 2:1 subharmonic range irregular oscillatory stripes and cluster patterns are found.

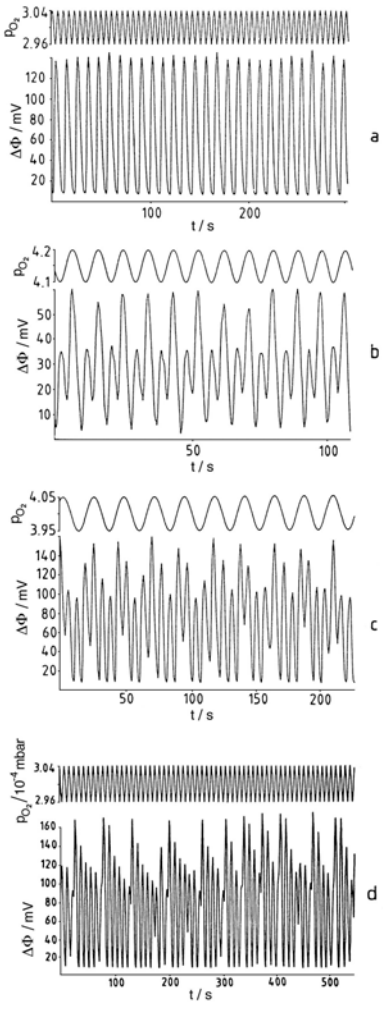

Fig. 24: Time series for periodically forced oscillations in the CO oxidation on a Pt(110) surface exhibiting sustained oscillations with frequency ν_0. Modulation of p_{O2} with frequency ν_p and amplitude A (as percentage of the basic value): (a) 1:2 subharmonic entrainment, $\nu_0 = 0.09\ s^{-1}$, $\nu_p = 0.18\ s^{-1}$, $A = 1.2\%$; (b) 2:1 superharmonic entrainment, $\nu_0 = 0.25\ s^{-1}$, $\nu_p = 0.11\ s^{-1}$, $A = 1.2\%$; (c) 7:2 superharmonic entrainment, $\nu_0 = 0.185\ s^{-1}$, $\nu_p = 0.047\ s^{-1}$, $A = 1.2\%$; (d) quasiperiodic behavior, $\nu_0 = 0.25\ s^{-1}$, $\nu_p = 0.016\ s^{-1}$, $A = 1.2\%$ [22].

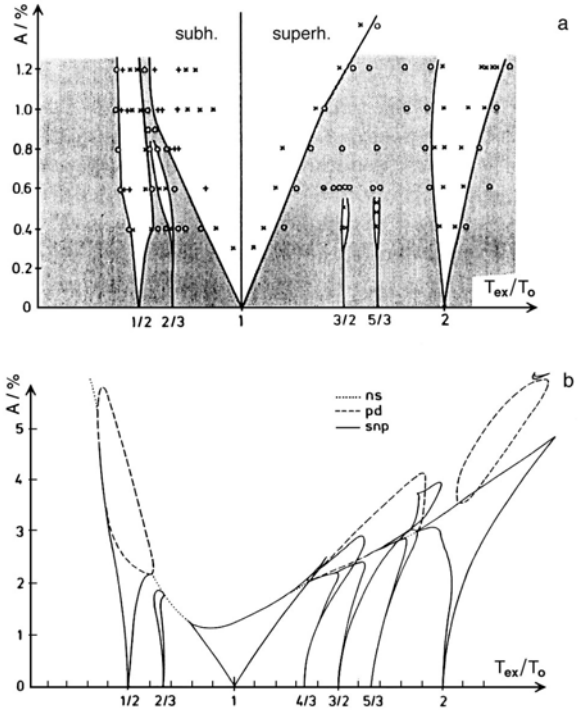

Fig. 25: Dynamic phase diagram for periodically forced oscillations in the CO oxidation on a Pt(110) surface. Existence range for entrained and quasiperiodic oscillations as a function of the period ratio of modulation and autonomous oscillations, T_{ex} / T_0, and of the amplitude (as percentage of the base pressure) of the modulated O_2 partial pressure. (a) Experimental results, where shaded areas indicate conditions for quasiperiodic behavior between the sub- and superharmonic entrainment bands [22]. (b) Theoretical result, obtained with the quoted system of differential equations modeling the kinetics. Types of bifurcation: ns = Neimark-Sacker, pd = period doubling, snp = saddle node [259].

If the autonomous system itself is in a chaotic rather than periodic state, control of this spatiotemporal chaos becomes a more sophisticated task which could be solved by applying a strategy of delayed feedback [261]. With the CO oxidation reaction on Pt(110) spatio-temporal patterns were continuously recorded by PEEM images whose integrated intensities reflected the (integral) state of the surface. This signal was then used to adjust the flow of CO with a certain strength and delay time as parameters. When feedback intensity was increased, spiral-wave turbulence was transformed into new intermittent chaotic regimes. For other sets of parameters the development of cluster patterns and of standing waves or even stabilization of spatially uniform oscillations was observed. In a more refined feedback scheme the coupling protocol is adjusted to the properties of the existing pattern which enables even more sensitive and efficient control [262]. As example, Fig. 26 shows the evolution of bubble shaped concentration patterns emerging periodically under the influence of such a nonuniform coupling scheme.

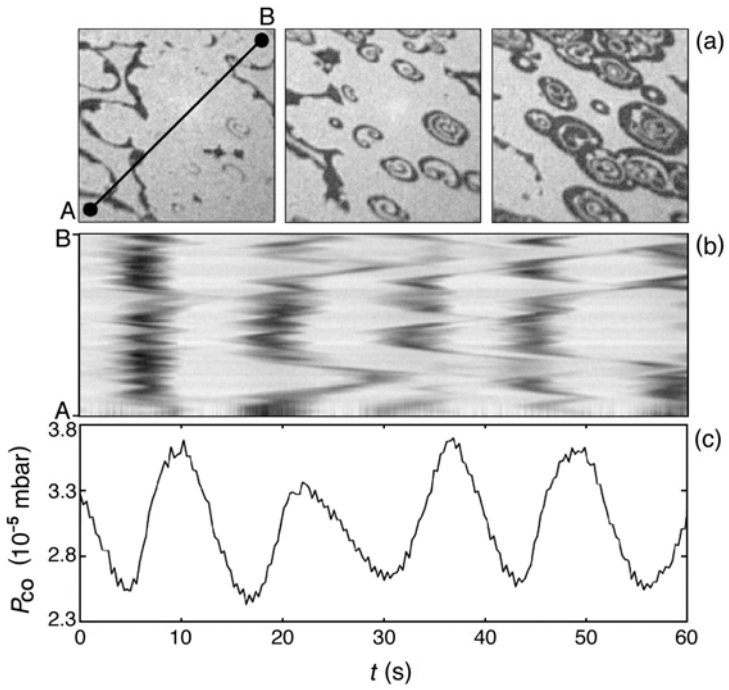

Fig. 26: Pattern formation in CO oxidation on Pt(110) subject to nonuniform coupling as reflected by the modulation of the CO partial pressure around p^{o}_{CO} = 2.8 x 10^{-5} mbar at T = 453 K, p_{O_2} = 4 x 10^{-4} mbar (c). (a) shows 3 typical PEEM images recorded during one evolution cycle. (b) is a space-time diagram along the line A – B in (a).

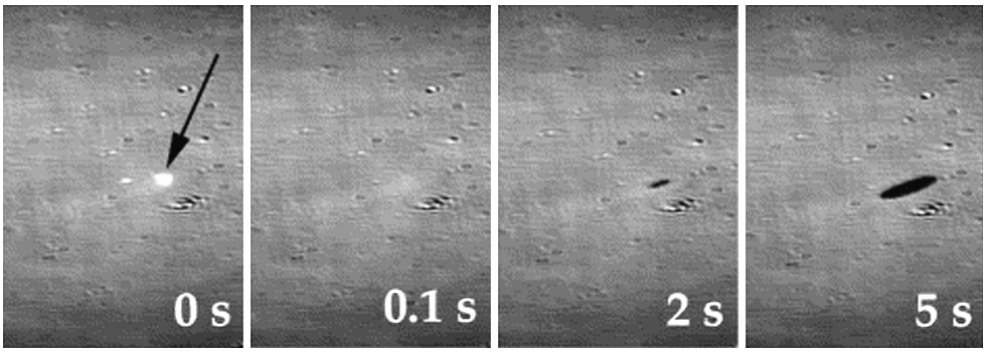

Fig. 27: A series of EMSI images (0.8 x 1.1 mm^2) from a Pt(110) surface during CO oxidation at p_{O_2} = 3 x 10^{-4} mbar, p_{CO} = 5.3 x 10^{-5} mbar, T = 473 K. the point marked by an arrow is irradiated for 90 ms by a laser shot causing local CO desorption, enabling oxygen adsorption and the ignition of a reaction zone.

Instead of varying one of the global parameters as a next step one can also think of its localized control. This could be achieved by focusing a laser beam into a narrow spot (~80 μm diameter) on the surface and by adjusting this spot through the computer controlled galvanometer mirrors within 5 μm on a time scale of 1 ms. In this way the local temperature could be increased typically by about 3 K thus affecting the local kinetics and thereby pattern formation [263]. This technique allows the local manipulation of catalytic activity, for example as shown in Fig. 27 for a single-shot ignition experiment [264]: Under the chosen steady-state flow conditions in the CO oxidation on Pt(110) the surface is largely covered by CO. Local heating causes partial CO desorption and adsorption of O_2, so that a reaction wave (dark spot) may develop and propagate. Apart from wave initiation [265] also the motion of already propagating reaction waves ('dragging') [266] may be affected, but also the overall reaction rate may be improved by controlled motion of the laser beam across the catalyst surface [267].

References

1. G. Nicolis, I. Prigogine, *Self-Organization in Non-Equilibrium Systems,* Wiley, New York, **1977**.
2. A. S. Mikhailov, *Foundations of Synergetics,* Springer, Berlin, **1991**, Vols I and II.
3. U. F. Franck, *Ber. Bunsenges. Phys. Chem.* **1980**, *84*, 334.
4. A. M. Zhabotinsky, *Ber. Bunsenges. Phys. Chem.* **1980**, *84*, 303.
5. R. J. Field, M. Burger (Eds), *Oscillations and Travelling Waves in Chemical Systems, Wiley, New York,* **1985**.
6. P. Hugo, *Ber. Bunsenges. Phys. Chem.* **1970**, 74, 121.
7. H. Beusch, D. Fieguth, E. Wicke, *Chem. Ing. Techn.* **1972**, *44*, 445.
8. M. Sheintuch, R. A. Schmitz, *Catal. Rev.-Sci. Eng.* **1977**, *15*, 107.
9. M. G. Slinko, M. M. Slinko, *Catal. Rev.-Sci Eng.* **1978**, *17*, 119.
10. L. F. Razon, R. A. Schmitz, *Catal. Rev.-Sci. Eng.* **1986**, *28*, 89.
11. G. Ertl, *Adv. Catal.* **1990**, *37*, 213.
12. R. Imbihl, *Progr. Surf. Sci.* **1993**, *44*, 185.
13. F. Schüth, B. E. Henry, L. D. Schmidt, *Adv. Catal.* **1993**, *39*, 51.
14. M. M. Slinko, N. Jaeger, *Oscillating Heterogeneous Catalytic Systems,* Elsevier, Amsterdam, **1994**.
15. R. Imbihl, G. Ertl, *Chem. Rev.,* **1995**, *95*, 697.
16. M. Eiswirth, G. Ertl in *Chemical Waves and Patterns* (Eds: R. Kapral, K. Showalter), Kluwer, Dordrecht, **1994**, 447.
17. Special issue of *Catal. Today* (Eds. M. Slinko, H. Jaeger) **2005** (in print).
18. J. Lauterbach, G. Haas, H. H. Rotermund, G. Ertl, *Surf. Sci.* **1993**, *294*, 116.
19. M. F. H. van Tol, A. Gielbert, B. E. Nieuwenhuys, *Catal. Lett.* **1992**, *16*, 297.
20. V. Gorodetskii, J. H. Block, W. Drachsel, M. Ehsasi, *Appl. Surf. Sci.* **1993**, *67*, 198.
21. M. Ehsasi, O. Frank, J. H. Block, K. Christmann, *Chem. Phys. Lett.* **1990**, *165*, 115.
22. M. Eiswirth, G. Ertl, *Phys. Rev. Lett.* **1988**, *60*, 1526.
23. J. W. Döbereiner, *Schweigg. J.* **1823**, *39,* 1
24. S. Völkening, K. Bedürftig, K. Jacobi, J. Wintterlin, G. Ertl, *Phys. Rev. Lett.* **1999**, *83,* 2672.
25. C. Clay, S. Haq, A. Hodgsen, *Phys. Rev. Lett.* **2004**, *92,* 046102.
26. A. Michaelides, P. Hu, *J. Chem.. Phys.* **2001**, *114,* 513.
27. G. S. Karlberg, F. E. Olson, M. Persson, G. Wahnstrom, *J. Chem. Phys.* **2003**, *119,* 4865.
28. C. Sachs, M. Hildebrand, S. Völkening, J. Wintterlin, G. Ertl, *Science* **2001**, *293,* 1635.
29. V. P. Zhdanov, *Phys. Rev. E* **1999**, *59,* 6292; *60,* 7554.
30. V. P. Zhdanov, B. Kasemo, *J. Statis. Phys.* **2000**, *101,* 631.

31. V. P. Zhdanov, *Surf. Sci. Rep.* **2002**, *45,* 233.
32. J. Guckenheimer, P. Holmes, *Nonlinear Dynamics, Dynamical Systems, and Bifurcations of Vector Fields,* Springer, Berlin, **1986**.
33. J. M. T. Thompson, H. B. Stewart, *Nonlinear Dynamics and Chaos*, Wiley, New York, **1987**.
34. M. Eiswirth, A. Freund, J. Ross, *J. Phys. Chem.* **1991**, *95*, 1294.
35. M. Eiswirth, A. Freund, J. Ross, *Adv. Chem. Phys.* **1991**, *80*, 127.
36. G. Eigenberger, *Chem. Eng. Sci.* **1978**, *33*, 1263.
37. V. D. Belyav, M. M. Slinko, V. L. Timoshenko, M. G. Slinko, *Kinet. Katal.* **1973**, *14*, 810.
38. C. A. Pikio, D. Luss, *Chem. Eng. Sci.* **1977**, *32*, 191.
39. I. G. Kevrekidis, L. D. Schmidt, R. Aris, *Surf. Sci.* **1984**, *137*, 151.
40. S. S. Tambe, V. R. Kumar, K. N. Ponnani, B. D. Kulkarni, *Chem. Eng. J.* **1987**, *34*, 143.
41. D. G. Vlachos, L. D. Schmidt, R. Aris, *J. Chem. Phys.* **1990**, *93*, 8306.
42. C. G. Takoudis, L. D. Schmidt, R. Aris, *Surf. Sci.* **1981**, *105*, 325.
43. M. A. McKarnin, R. Aris, L. D. Schmidt, *Proc. Roy. Soc. A* **1988**, **415**, 363.
44. A. Winfree, *When Time Breaks Down*, Princeton University Press, Princeton, **1987**.
45. H. Swinney, V. I. Krinsky (Eds), *Wave Patterns in Chemical and Biological Systems*, Physica D **1991**, 49.
46. A. V. Holden, M. Markus, H. G. Othmer (Eds), *Nonlinear Wave Processes in Excitable Media*, Plenum Press, New York, **1991**.
47. R. Luther, *Z. Elektrochem.* **1906**, *12*, 596.
48. A. M. Turing, *Phil. Trans. Roy. Soc. B* **1952**, *237*, 37.
49. J. Falta, R. Imbihl, M. Henzler, *Phys. Rev. Lett.* **1990**, *64*, 1409.
50. R. Imbihl, A. E. Reynolds, D. Kaletta, *Phys. Rev. Lett.* **1991**, *67*, 275.
51. M. Bär, C. Zülicke, M. Eiswirth, G. Ertl, *J. Chem. Phys.* **1992**, *96*, 8595.
52. J. P. Keener, J. J. Tyson, *Physica D* **1986**, *21*, 300.
53. A. S. Mikhailov, V. S. Zykov, *Physica D* **1991**, *52*, 379.
54. M. Sheintuch, *Chem. Eng. Sci.* **1981**, *36*, 893.
55. F. Mertens, R. Imbihl, A. S. Mikhailov, *J. Chem. Phys.* **1993**, *99*, 8668.
56. J. L. Lumley, *Stochastic Tools in Turbulence*, Academic Press, New York, **1970**.
57. M. D. Graham, S. L. Lane, D. Luss, *J. Phys. Chem.* **1993**, *97*, 889.
58. K. Krischer, R. Rico-Martinez, I. Kevrekidis, H. H. Rotermund, G. Ertl, J. L. Hudson, *AIChE J.* **1993**, *39*, 89.
59. G. Ertl, P. R. Norton, J. Rüstig, *Phys. Rev. Lett.* **1982**, *49*, 177.
60. T. Engel, G. Ertl, *Adv. Catal.* **1979**, *28*, 1.
61. J. Wintterlin, S. Völkening, T. V. W. Janssens, T. Zambelli, G. Ertl, *Science* **1997**, *278,* 1931
62. R. Imbihl, M. Sander, G. Ertl, *Surf. Sci.* **1988**, *204*, L 701.
63. S. Oh, G. B. Fisher, J. E. Carpenter, D. W. Goodman, *J. Catal.* **1986**, *100*, 360.
64. E. Wicke, P. Kummann, W. Keil, J. Schiefler, *Ber. Bunsenges. Phys. Chem.* **1980**, *84*, 315.
65. M. Ehsasi, M. Matloch, O. Frank, J. H. Block, K. Christmann, F. Rys, W. Hirschwald, *J. Chem. Phys.* **1989**, *91*, 4949.
66. K. Krischer, M. Eiswirth, G. Ertl, *J. Chem. Phys.* **1992**, *96*, 9161.
67. V. P. Zhdanov, B. Kasemo, *Surf. Sci. Rep.* **1994**, *20*, 111.
68. M. P. Cox, G. Ertl, R. Imbihl, *Phys. Rev. Lett.* **1985**, *54*, 1725.
69. M. Eiswirth, G. Ertl, *Surf. Sci.* **1986**, *177*, 90.
70. M. Ehsasi, S. Rezaie-Serej, J. H. Block, K. Christmann, *J. Chem. Phys.* **1990**, *92*, 7596.
71. M. Sander, R. Imbihl, G. Ertl, *J. Chem. Phys.* **1991**, *95*, 6162.
72. S. R. Bare, P. Hoffmann, D. A. King, *Surf. Sci.* **1984**, *144*, 347.
73. T. E. Jackman, J. A. Davies, D. P. Jackson, W. N. Unertl, P. R. Norton, *Surf. Sci.* **1982**, *120*, 389.

74. T. Gritsch, D. Coulman, R. J. Behm, G. Ertl, *Phys. Rev. Lett.* **1989**, *63*, 1086.

75. N. Freyer, M. Kiskinova, G. Pirug, H. P. Bonzel, *Surf. Sci.* **1986**, *166*, 206.

76. M. Eiswirth, K. Krischer, G. Ertl, *Surf. Sci.* **1988**, *202*, 565.

77. M. Eiswirth, T. M. Kruel, G. Ertl, F. W. Schneider, *Chem. Phys. Lett.* **1992**, *193*, 305.

78. M. Falcke, M. Bär, H. Engel, M. Eiswirth, *J. Chem. Phys.* **1992**, *97*, 4555.

79. M. Bär, N. Gottschalk, M. Eiswirth, G. Ertl, *J. Chem. Phys.* **1994**, *100*, 1202.

80. H. H. Rotermund, S. Jakubith, A. von Oertzen, S. Kubala, G. Ertl, *J. Chem. Phys.* **1989**, *91*, 4942.

81. F. Esch, S. Günther, E. Schütz, A. Schaak, I. G. Kevrekidis, M. Marsi, M. Kiskinova, R. Imbihl, *Catal. Lett.* **1998**, *52,* 85.

82. H. Marbach, M. Hinz, S. Günther, L. Gregoratti, M. Kiskinova, R. Imbihl, *Chem. Phys. Lett.* **2002**, *364,* 207.

83. W. Engel, M. Kordesch, H. H. Rotermund, S. Kubala, A. von Oertzen, *Ultramicroscopy* **1991**, *95*, 6162.

84. W. Swiech, B. Rausenberger, W. Engel, A. M. Bradshaw, E. Zeitler, *Surf. Sci.* **1993**, *294*, 297.

85. W. Swiech, C. S. Rastomjee, R. Imbihl, J. W. Evans, B. Rausenberger, W. Engel, A. K. Schmidt, A. M. Bradshaw, E. Zeitler, *Surf. Sci.* **1994**, *307*, 138.

86. K. C. Rose, W. Engel, F. Meissen, A. J. Patchett, A. M. Bradshaw, R. Imbihl, *Surf. Rev. Lett.* **1998**, *5*, 1233.

87. F. Meissen, A. J. Patchett, R. Imbihl, A. M. Bradshaw, *Chem. Phys. Lett.* **2001**, *336,* 181.

88. H. H. Rotermund, G. Haas, R. U. Franz, R. M. Tromp, G. Ertl, *Science* **1995**, *270,* 608.

89. S. Nettesheim, A. von Oertzen, H. H. Rotermund, G. Ertl, *J. Chem. Phys.* **1993**, *98*, 9977.

90. A. von Oertzen, H. H. Rotermund, S. Nettesheim, *Surf. Sci.* **1994**, *311*, 322.

91. A. Schaak, S. Shaikhutdinov, R. Imbihl, *Surf. Sci.* **1998**, *421,* 191.

92. M. Tammaro, J. W. Evans, C. S. Rastamjee, W. Swiech, A. M. Bradshaw, R. Imbihl, *Surf. Sci.* **1998**, *407,* 162.

93. M. Bär, M. Eiswirth, *Phys. Rev. E* **1993**, *48*, R 1635.

94. S. Jakubith, H. H. Rotermund, W. Engel, A. von Oertzen, G. Ertl, *Phys. Rev. Lett.* **1990**, *65*, 3013.

95. H. H. Rotermund, S. Jakubith, A. von Oertzen, G. Ertl, *Phys. Rev. Lett.* **1991**, *66*, 3083.

96. M. Bär, M. Eiswirth, H. H. Rotermund, G. Ertl, *Phys. Rev. Lett.* **1992**, *69*, 945.

97. M. Eiswirth, P. Möller, K. Wetzl, R. Imbihl, G. Ertl, *J. Chem. Phys.* **1988**, *90*, 510.

98. M. Falcke, H. Engel in *Spatio-Temporal Organization in Nonequilibrium Systems* (Eds: S. C. Müller, T. Plesser), Projektverlag, Dortmund, **1992**.

99. H. Levine, X. Zhou, *Phys. Rev. E* **1993**, *48*, 50.

100. A. von Oertzen, H. H. Rotermund, A. S. Mikhailov, G. Ertl, *J. Phys. Chem. B* **2000**, *104,* 3155.

101. P. R. Norton, P. E. Bindner, K. Griffiths, T. E. Jackman, J. A. Davies, J. Rüstig, *J. Chem. Phys.* **1984**, *80*, 3859.

102. R. Imbihl, M. P. Cox, G. Ertl, *J. Chem. Phys.* **1986**, *84*, 3519.

103. R. Imbihl, M. P. Cox, G. Ertl, H. Müller, W. Brenig, *J. Chem. Phys.* **1985**, *83*, 1578.

104. P. Möller, K. Wetzl, M. Eiswirth, G. Ertl, *J. Chem. Phys.* **1986**, *85*, 5328.

105. R. J. Behm, P. A. Thiel, P. R. Norton, G. Ertl, *J. Chem. Phys.* **1983**, *78*, 7438; 7448.

106. K. Heinz, E. Lang, K. Strauss, K. Müller, *Appl. Surf. Sci.* **1982**, *11/12*, 611.

107. P. R. Norton, J. A. Davies, D. K. Geber, C. W. Sitter, T. E. Jackman, *Surf. Sci.* **1981**, *108*, 205.

108. A. Crossley, D. A. King, *Surf. Sci.* **1980**, 95, 131.

109. A. Hopkinson, J. M. Bradley, X. C. Guo, D. A. King, *Phys. Rev. Lett.* **1993**, *71*, 1597.

110. P. R. Norton, K. Griffiths, P. E. Bindner, *Surf. Sci.* **1984**, *138*, 125.

111. X. C. Guo, A. T. Pasteur, D. A. King, *Surf. Sci.*, in press.

112. I. M. Irurzun, R. B. Hoyle, M. R. E. Proctor, D. A. King, *Chem. Phys. Lett.* **2003**, *377,* 269.

113. S. Ladas, R. Imbihl, G. Ertl, *Surf. Sci.* **1988**, *197*, 1153; *198*, 42.

114. M. Sander, R. Imbihl, G. Ertl, *J. Chem. Phys.* **1992**, *97*, 5193.

115. M. Sander, R. Imbihl, R. Schuster, J. V. Barth, G. Ertl, *Surf. Sci.* **1992**, *281*, 159.

116. M. Ehsasi, C. Seidel, H. Ruppender, W. Drachsel, J. H. Block, K. Christmann, *Surf. Sci.* **1989**, *210*, L 198.

117. S. Ladas, R. Imbihl, G. Ertl, *Surf. Sci.* **1989**, *219*, 88.

118. M. Ehsasi, O. Frank, J. H. Block, K. Christmann, *Chem. Phys. Lett.* **1990**, *165*, 115.

119. M. Ehsasi, M. Berdau, T. Rebitzki, K. P. Charlé, K. Christmann, J. H. Block, *J. Chem. Phys.* **1993**, *98*, 9177.

120. M. R. Bassett, R. Imbihl, *J. Chem. Phys.* **1990**, *93*, 811.

121. M. Berdau, M. Ehsasi, A. Karpowicz, W. Engel, K. Christmann, J. H. Block, *Vacuum* **1994**, *45*, 271.

122. J. Witte, U. Memmert, K. Griffiths, P. R. Norton, *J. Chem. Phys.* **1989**, *90*, 5082; 5088.

123. M. Milun, P. Pervan, M. Vajic, K. Wandelt, *Surf. Sci.* **1989**, *211/212*, 887.

124. H. H. Rotermund, J. Lauterbach, G. Haas, *Appl. Phys. A* **1993**, *57*, 507.

125. J. Lauterbach, K. Asakura, H. H. Rotermund, *Surf. Sci.* **1994**, *313*, 52.

126. J. E. Turner, M. B. Maple, *Surf. Sci.* **1984**, *147*, 647.

127. 107. B. C. Sales, J. E. Turner, M. B. Maple, *Surf. Sci.* **1982**, *114*, 381.

128. D. J. Kaul, E. E. Wolf, *J. Catal.* **1985**, *91*, 216.

129. T. Lindstrom, T. T. Tsotsis, *Surf. Sci.* **1985**, *150*, 487.

130. I. V. Yentakakis, C. G. Vayenas, *J. Catal.* **1989**, *111*, 170.

131. N. Hartmann, R. Imbihl, W. Vogel, *Catal. Lett.* **1994**, *28*, 373.

132. R. C. Yeates, J. E. Turner, A. J. Gellmann, G. A. Somorjai, *Surf. Sci.* **1985**, *149*, 175.

133. P. A. Carlsson, V. P. Zhdanov, B. Kasemo, Appl. *Surf. Sci.* **2005**, *239*, 424.

134. V. A. Burrows, S. Sundaresan, Y. J. Chabal, S. B. Christmann, *Surf. Sci.* **1987**, *180*, 110.

135. V. A. Burrows, S. Sundaresan, Y. J. Chabal, S. B. Christmann, *Surf. Sci.* **1985**, *160*, 122.

136. H. U. Onken, E. Wicke, *Ber. Bunsenges. Phys. Chem.* **1986**, *90*, 976.

137. M. M. Slinko, N. I. Jaeger, P. Svensson, *J. Catal.* **1989**, *118*, 349.

138. L. F. Razon, S. M. Chang, R. A. Schmitz, *Chem. Eng. Sci.* **1986**, *41*, 1561.

139. J. Kapicka, M. Marek, *Surf. Sci.* **1989**, *222*, L 885.

140. W. Adlhoch, H. G. Lintz, T. Weisker, *Surf. Sci.* **1981**, *103*, 576.

141. 5. P. Singh-Boparai, D. A. King, *Proc. 4th Int. Congr. Surf. Sci.*, Cannes, **1980**, p. 403.

142. S. B. Schwartz, L. D. Schmidt, *Surf. Sci.* **1987**, *183*, L 269.

143. 5. B. Schwartz, L. D. Schmidt, *Surf. Sci.* **1988**, *206*, 169.

144. T. Fink. J. P. Dath, R. Imbihl, G. Ertl. *J. Chem. Phys.* **1991**, *95*, 2109.

145. J. P. Dath, T. Fink, R. Imbihl, G. Ertl, *J. Chem. Phys.* **1992**, *96*, 1582.

146. G. Veser, R. Imbihl, *J. Chem. Phys.* **1992**, *96*, 7155.

147. G. Veser, F. Mertens, A. S. Mikhailov, R. Imbihl, *Phys. Rev. Lett.* **1993**, *71*, 935.

148. G. Veser, R. Imbihl, *J. Chem. Phys.* **1994**, *100*, 8483; 8492.

149. M. W. Lesley, L. D. Schmidt, *Surf. Sci.* **1985**, *155*, 215.

150. T. Fink, J. P. Dath, M. R. Bassett, R. Imbihl, G. Ertl, *Surf. Sci.* **1991**, *245*, 96.

151. R. Imbihl, T. Fink, K. Krischer, *J. Chem. Phys.* **1992**, *96*, 6236.

152. A. Hopkinson, D. A. King, *Chem. Phys.* **1994**, 177.

153. Y. Uchida, R. Imbihl, G. Lehmpfuhl, *Surf. Sci.* **1992**, *275*, 253.

154. 154, V. P. Zhdanov, *Catal. Lett.* **2002**, *84,* 147.

155. J. Siera, P. Cobden, K. Tanaka, B. E. Nieuwenhuys, *Catal. Lett.* **1991**, *10*, 335.

156. M. Slinko, T. Fink, T. Löher, H. H. Madden, S. J. Lombardo, R. Imbihl, G. Ertl, *Surf. Sci.* **1992**, *264*, 157.

157. P. D. Cobden, J. Siera, B. E. Nieuwenhuys, *J. Vac. Sci. Technol. A* **1992**, *10*, 2487.

158. 158 C. A. de Wolf, B. E. Nieuwenhuys, *Catal. Today* **2001**, *70,* 287.

159. 159 N. M. H. Janssen, A. Schaak, B. E. Nieuwenhuys, R. Imbihl, *Surf. Sci.* **1996**, *364,* L555.

160. N. Khrustova, A. S. Mikhailov, R. Imbihl, *J. Chem. Phys.* **1997**, *107,* 2096.

161. 161 C. A. de Wolf, J. W. Bakker, P. T. Wonda, B. E. Nieuwenhuys, A. Baraldi, S. Lizzit, M. Kiskinova, *J. Phys. Chem. B* **2001**, *105,* 4254.

162. C. Voss, N. Kruse, *Ultramicroscopy* **1998**, *73,* 211.

163. 163 T. V. de Bocarme, N. Kruse, *Chaos* **2002**, *12,* 118.

164. 164 T. D. Chan, T. V. de Bocarme, N. Kruse, *Surf. and Interface Anal.* **2004**, *36,* 528.

165. 165 M. Gruyters, A. T. Pasteur, D. A. King, *Faraday Trans.* **1996**, *92,* 2941.

166. 166 A. v. Walker, M. Gruyters, D. A. King, *Surf. Sci.* **1999**, *384,* L791.

167. 167 V. P. Zhdanov, B. Kasemo, *Appl. Catal. A* **1999**, *187,* 61.

168. 168 I. M. Irurzun, R. Imbihl, J. L. Ficento, E. E. Mola, *Chem. Phys. Lett.* **2004**, *389,* 212.

169. C. G. Takoudis, L. D. Schmidt, *J. Phys. Chem.* **1983**, *87*, 958; 964.

170. T. Katona, G. A. Somorjai, *J. Phys. Chem.* **1992**, *96*, 5465.

171. S. J. Lombardo, F. Esch, R. Imbihl, *Surf. Sci.* **1992**, *271*, L 367.

172. M. F. H. van Tol, J. Siera, P. D. Cobden, B. E. Nieuwenhuys, *Surf. Sci.* **1992**, *274*, 63.

173. S. J. Lombardo, T. Fink, R. Imbihl, *J. Chem. Phys.* **1993**, *98*, 5526.

174. G. Veser, F. Esch, R. Imbihl, *Catal. Lett.* **1992**, *13*, 371.

175. M. F. H. van Tol, J. de Maaijoe-Gielbert, B. E. Nieuwenhuys, *Chem. Phys. Lett.* **1993**, *205*, 207.

176. F. Mertens, R. Imbihl, *Nature* **1994**, *370*, 124.

177. N. Gottschalk, F. Mertens, M. Bär, M. Eiswirth, R. Imbihl, *Phys. Rev. Lett.* **1994**, *73*, 3483.

178. B. Hellsing, B. Kasemo, V. P. Zhdanov, *J. Catal.* **1991**, *132*, 210.

179. J. K. Gimzewskii, C. Gerber, E. Meyer, R. R. Schiller, *Chem. Phys. Lett.* **1994**, 217, 289.

180. V. P. Zhdanov, *Surf. Sci.* **1993**, *296*, 261.

181. V. Gorodetskii, J. Lauterbach, H. H. Rotermund, J. H. Block, G. Ertl, *Nature* 1994, *370*, 277.

182. V. Barelko, I. I. Kurachka, A. G. Merzhanao, K. G. Shkadinskii, *Chem. Eng. Sci.* **1978**, *33*, 805.

183. J. C. Kellow, E. E. Wolf, *Chem. Eng. Sci.* **1990**, *45*, 2597.

184. F. Quin, E. E. Wolf, A. C. Chang, *Phys. Rev. Lett.* **1994**, *72*, 1459.

185. R. Sant, E. E. Wolf, *J. Catal.* **1988**, *110*, 210.

186. C. C. Chan, E. E. Wolf; H. C. Chang, *J. Phys. Chem.* **1993**, *97*, 1055.

187. H. U. Onken, E. Wicke, *Ber. Bunsenges. Phys. Chem.* **1986**, *90*, 976.

188. H. U. Onken, E. Wicke, *Z. Phys. Chem. NF* **1989**, *165*, 23.

189. J. P. Dath, J. P. Dauchot, *J. Catal.* **1989**, *115*, 593.

190. P. K. Tsai, M. B. Maple, R. K. Hers, *J. Catal.* **1988**, *112*, 453.

191. 191 F. Cirak, J. E. Cisternas, A. M. Cuitino, G. Ertl, P. Holmes, I. G. Kevrekidis, M. Ortiz, H. H. Rotermund, H. Schunack, J. Wolf, *Science* **2003**, *300,* 1932.

192. S. A. Zhukov, V. Barelko, *Sov. J. Chem. Phys.* **1982**, *1*, 883.

193. Yu. E. Volodin, V. Barelko, A. G. Merzhanov, *Sov. J. Chem. Phys.* **1982**, *1*, 1146.

194. L. Lobban, D. Luss, *J. Phys. Chem.* **1989**, *93*, 6530.

195. L. Lobban, G. Philippou, D. Luss, *J. Phys. Chem.* **1989**, *93*, 733.

196. G. Philippou, F. Schultz, D. Luss, *J. Phys. Chem.* **1991**, *95*, 3224.

197. G. Philippou, D. Luss, *J. Phys. Chem.* **1992**, *96*, 6651.

198. G. Philippou, D. Luss, *Chem. Eng. Sci.* **1993**, *48*, 2313.

199. G. A. Cordonnier, F. Schüth, L. D. Schmidt, *J. Chem. Phys.* **1989**, *91*, 5374.

200. M. Sheintuch, *Chem. Eng. Sci.* **1989**, *44*, 1081.

201. M. Sheintuch, *J. Phys. Chem.* **1990**, *94*, 5889.

202. S. L. Lane, D. Luss, *Phys. Rev. Lett.* **1993**, *70*, 830.

203. M. D. Graham, S. L. Lane, D. Luss, *J. Chem. Phys.* **1993**, *97*, 7564.

204. R. A. Schmitz, G. A. D'Netto, L. F. Razon, J. R. Brown in *Chemical Instabilities* (Eds: G. Nicolis, F. Baras), Dordrecht, Amsterdam, **1989**.

205. P. C. Pawlicki, R. A. Schmitz, *Chem. Eng. Progr.* **1987**, *83*, 40.

206. M. D. Graham, S. L. Lane, D. Luss, *J. Chem. Phys.* **1993**, *97*, 889.

207. M. Sheintuch, *J. Catal.* **1985**, *96*, 326.

208. R. Dagonnier, M. Dumont, J. Nuyts, *J. Catal.* **1980**, *66*, 130.

209. F. Schüth, E. Wicke, *Ber. Bunsenges. Phys. Chem.* **1989**, *93*, 491.

210. H. C. Chang, M. Aluko, *Chem. Eng. Sci.* **1984**, *39*, 36; 51.

211. M. Aluko, H. C. Chang, *Chem. Eng. Sci.* **1986**, *41*, 317.

212. M. P. Harold, M. Sheintuch, D. Luss, *I & EC Research* **1987**, *26*, 786; 795; 1616.

213. S. A. Zhukov, V. Barelko, *Dokl. Akad. Nauk SSSR* **1978**, *238*, 135.

214. Yu. E. Volodin, V. N. Zuyagin, A. N. Ivanova, V. Barelko, *Adv. Chem. Phys.* **1990**, *77*, 551.

215. O. Middaya, M. D. Graham, D. Luss, M. Sheintuch, *J. Chem. Phys.* **1993**, *98*, 2823.

216. U. Middya, M. Sheintuch, M. D. Graham, D. Luss, *Physica D* **1993**, *63*, 393.

217. U. Middya, D. Luss, M. Sheintuch, *J. Chem. Phys.* **1994**, *100*, 3568.

218. V. Barelko, E. C. Pechatnikov, A. N. Ivanova, *Sov. J. Chem. Phys.* **1991**, *7*, 1153.

219. H. Marbach, M. Hinz, S. Günther, L. Gregoratti, M. Kiskinova, R. Imbihl, *Chem. Phys. Lett.* **2002**, *364,* 207.

220. H. Marbach, S. Günther, B. Luerssen, L. Gregoratti, M. Kiskinova, R. Imbihl, *Catal. Lett.* **2002**, *83,* 161.

221. K. Asakura, J. Lauterbach, H. H. Rotermund, G. Ertl, *Phys. Rev. B* **1994**, *50,* 8043.

222. K. Asakura, J. Lauterbach, H. H. Rotermund, G. Ertl, *Surf. Sci.* **1997**, *374,* 125.

223. 223 P. Manneville, *Dissipative Structures and Weak Turbulence*, Academic Press, London, **1990**.

224. A. Babloyantz, J. A. Sepulchre, *Physica D* **1991**, *49*, 52.

225. J. Enderlein, *Phys. Lett.* **1991**, *156*, 429.

226. M. D. Graham, I. G. Kevrekidis, K. Asakura, J. Lauterbach, K. Krischer, H. H. Rotermund, G. Ertl, *Science* **1994**, *264*, 80.

227. E. Schütz, N. Hartmann, I. G. Kevrekidis, R. Imbihl, *Faraday Disc.* **1996**, *165,* 47.

228. E. Schütz, N. Hartmann, I. G. Kevrekidis, R. Imbihl, *Catal. Lett.* **1998**, *54,* 181.

229. S. Y. Shvartsman, E. Schütz, R. Imbihl, I. G. Kevrekidis, *Catal. Today* **2001**, *70,* 301.

230. J. Lauterbach, H. H. Rotermund, P. B. Rasmussen, M. Bär, M. D. Graham, I. G. Kevrekidis, G. Ertl, *Physica D* **1998**, *123,* 493.

231. 231 E. Schütz, F. Esch, S. Günther, A. Schaak, M. Marsi, M. Kiskinova, R. Imbihl, *Catal. Lett.* **1999**, *63,* 13.

232. F. Esch, S. Günther, E. Schütz, A. Schaak, I. G. Kevrekidis, M. Marsi, M. Kiskinova, R. Imbihl, *Catal. Lett.* **1998**, *52,* 85.

233. V. P. Zhdanov, B. Kasemo, *Physica D* **2001**, *151,* 73.

234. M. Lawin, V. Johanek, A. W. Grant, B. Kasemo, J. Libuda, H. J. Freund, *J. Chem. Phys.* **2005**, *122,* 084713.

235. J. W. Evans, *Langmuir* **1991**, *7*, 2514.

236. 236. R. M. Ziff, E. Gulari, Y. Barshed, *Phys. Rev. Lett.* **1986**, *56*, 2553.

237. P. Möller, K. Wetzel, M. Eiswirth, G. Ertl, *J. Chem. Phys.* **1986**, *85*, 5328.

238. X. G. Wu, R. Kapral, *Physica A* **1992**, *188*, 284.

239. A. S. Mikhailov, G. Ertl, *Chem. Phys. Lett.* **1995**, *238*, 104.

240. W. C. Conner, G. M. Pajonk, S. J. Teichner, *Adv. Catal.* **1986**, *34*, 1.

241. V. P. Zhdanov, B. Kasemo, *Surf. Sci. Rep.* **2000**, *39,* 29.

242. H. Persson, P. Thormalen, V. p. Zhdanov, B. Kasemo, *J. Vac. Sci. Techn. A* **1999**, *17,* 1721.

243. V. P. Zhdanov, B. Kasemo, *Phys. Rev. E* **2000**, *61,* R2184.

244. V. P. Zhdanov, B. Kasemo, *J. Catal.* **2003**, *214,* 121.

245. V. P. Zhdanov, B. Kasemo, *Surf. Sci.* **2002**, *496,*

246. V. Johanek, M. Laurin, A. W. Grant, B. Kasemo, C. R. Henry, J. Libuda, *Science* **2004**, *304,* 1639.

247. Y. S. Matros in *Unsteady State Processes in Catalysis* (Ed: I. S. Matras), VSP, Utrecht, **1990**, p. 131.

248. L. L. Hegedus, C. C. Chang, D. J. McEwen, E. M. Sloan, *Ind. Eng. Chem. Fundam.* **1980**, *19*, 367.

249. M. B. Cutlip, C. J. Hawkins, D. Mukesh, W. Morton, C. N. Kenney, *Chem. Eng. Commun.* **1983**, *22*, 329.

250. G. Vaporciyan, A. Annapragada, E. Gulari, *Chem. Eng. Sci.* **1988**, *43*, 2457.

251. M. Marek in *Temporal Order* (Eds: L, Rensing, N. I. Jaeger), Springer, Heidelberg, **1985**.

252. D. L. Silveston, R. R. Hudgins, A. Renken, *Catal. Today* **1995**, *25,* 91.

253. P. Koci, M. Kubicek, M. Marek, *Catal. Today* **2004**, *98,* 345.

254. V. P. Zhdanov, *Surf. Sci. Rep.* **2004**, *55,* 1.

255. W. Vance, G. E. Tsahouras, J. Ross, *Progr. Theor. Phys.* **1989**, *99*, 331.

256. G. E. Tsahouras, J. Ross, *J. Chem. Phys.* **1987**, *87*, 6538; **1989**, *89*, 5715.

257. G. E. Tsahouras, J. Ross, *J. Phys. Chem.* **1989**, *93*, 2833.

258. R. Schwankner, M. Eiswirth, P. Möller, K. Wetzl, G. Ertl, *J. Chem. Phys.* **1987**, *87*, 742.

259. K. Krischer, M. Eiswirth, G. Ertl, *J. Chem. Phys.* **1992**, *97*, 307.

260. M. Bertram, C. Beta, H. H. Rotermund, G. Ertl, *J. Phys. Chem. B* **2003**, *107,* 9610.

261. M. Kim, M. Bertram, M. Pollmann, A. von Oertzen, A. S. Mikhailov, H. H. Rotermund, G. Ertl, *Science* **2001**, *292,* 1357.

262. C. Beta, M. G. Moula, A. S. Mikhailov, H. H. Rotermund, G. Ertl, *Phys. Rev. Lett.* **2004**, *93,* 188302.

263. J. Wolff, A. G. Papathanasiou, I. G. Kevrekidis, H. H. Rotermund, G. Ertl, *Science* **2001**, *294,* 134.

264. J. Wolff, A. G. Papathanasiou, H. H. Rotermund, G. Ertl, X. Li, I. G. Kevrekidis, *J. Catal.* **2003**, *216,* 246.

265. J. Wolf, A. G. Papathanasiou, H. H. Rotermund, G. Ertl, M. A. Katsoulakis, X. Li, I. G. Kevrekidis, *Phys. Rev. Lett.* **2003**, *90,* 148301.

266. J. Wolff, A. G. Papathanasiou, H. h. Rotermund, G. Ertl, X. Li, I. G. Kevrekidis, *Phys. Rev. Lett.* **2003**, *90,* 018302.

267. 'A. G. Papathanasiou, J. Wolff, I. G. Kevrekidis, H H. Rotermund, G. Ertl, *Chem. Phys. Lett.* **2002**, *358,* 407.